Study of the influence of printing parameters on the residual stresses present in FFF printed parts

Amauri Joel Simão Couto

FEUP Supervisor: Prof. Pedro Sousa

INEGI Supervisors: Dr. Gonçalo Cipriano, Engr. Tiago Domingues

U. PORTO
FEUP FACULDADE DE ENGENHARIA
UNIVERSIDADE DO PORTO

Master in Mechanical Engineering

June 2023

Aos meus pais.

À minha irmã.

Resumo

O Fabrico aditivo é cada vez mais uma tecnologia de produção de relevo no contexto atual. Uma das desvantagens deste processo de fabrico é a ocorrência de fenómenos de tensões residuais associados aos distintos gradientes de temperatura e taxas de arrefecimento inerentes ao processo.

Este trabalho consistiu na produção de provetes por fabrico aditivo usando a tecnologia de *Fused Deposition Modeling* e subsequente estudo das tensões residuais existentes em função dos parâmetros de impressão usados, aplicando a técnica do Método do Furo Cego associado à Correlação Digital de Imagem.

Foi elaborado um *Design of Experiments* no qual se variou a temperatura de extrusão do filamento, a espessura das camadas de impressão e a velocidade, com o intuito de determinar a influência destes fatores na presença de tensões residuais nas peças a considerar. A utilização de extensómetros virtuais, capazes de medir pequenas deslocações nas superfícies dos provetes através da técnica da correlação digital de imagem foi capaz de proporcionar uma alternativa à utilização de rosetas de extensómetros tradicionais para este efeito.

Foi possível concluir que a interação entre a temperatura de extrusão e a taxa de alimentação é significativa tanto para a variação da tensão principal mínima como da máxima, enquanto que o termo independente da temperatura de extrusão e o quadrado do termo da taxa de alimentação mostraram ser significantes aquando da análise dos resultados referentes à tensão principal mínima.

Palavras-chave: Tensões residuais, Correlação Digital de Imagem, Método do furo cego, Fused Filament Fabrication, Fabrico aditivo de polímeros.

Abstract

Additive manufacturing has increasingly shown itself as a prominent manufacturing technology in the current context. One of the disadvantages of this manufacturing process is the occurrence of the residual stress phenomena associated with different temperature gradients and cooling rates inherent to the process.

This work consisted of producing test specimens using additive manufacturing with Fused Deposition Modeling technology and subsequently studying the residual stresses present based on the printing parameters used, applying the Blind Hole Method associated with Digital Image Correlation.

A Design of Experiments was developed, in which the filament extrusion temperature, layer height, and feed rate were varied in order to determine the influence of these factors on the presence of residual stresses in the parts under consideration. The use of virtual extensometers, capable of measuring small displacements on the specimen surfaces using digital image correlation, provided an alternative to the use of traditional strain gage rosettes for this purpose.

It was possible to conclude that the interaction between the extrusion temperature and the feed rate is significant for the variation of both the minimum and maximum principal stresses, while the independent extrusion temperature term and the square feed rate term proved to be significant when analyzing the results related to the minimum principal stress.

Keywords: Residual stresses, Digital Image Correlation, Blind Hole Method, Fused Filament Fabrication, Additive Manufacturing of Polymers.

Ackowledgements

Firstly, I would like to thank my supervisors, Dr. Pedro Sousa, Dr. Gonçalo Cipriano and Engr. Tiago Domingues for the guidance throughout these past 5 months, all the advice and feedback.

To all the collaborators at INEGI, for such a warm welcome, and for assisting me with everything I needed to complete my work.

To my family, for the unconditional support, the kind and understanding words, and for providing me with the tools I needed to end up where I am today.

To my friends, for the good moments, the extra motivation needed to overcome any hurdles and the ever-present fun.

Table of Contents

List of abbreviations vii
List of figures viii
List of Tables x
1. Introduction 1
1.1. Project motivation 1
1.2. Host institution 1
1.3. Project objectives 2
1.4. Project planning 2
1.5. Dissertation structure 2
2. Literature review 3
2.1. Residual stresses 3
2.2. Influence of Residual Stresses on components 4
2.3. Hole Drilling method 7
2.4. Additive manufacturing 13
2.4.1. Fused Filament Fabrication 14
2.4.2. Material 16
2.5. Digital Image Correlation 17
2.6. Response surface Methodology 18
2.6.1. Central Composite Design 19
3. Methodology 21
3.1. Integral method 27
4. Results 29
4.1. Comparison between Traditional and DIC approaches 29
4.2. DoE Results 35
4.2.1. Statistical significance between the response and the terms 35
4.2.2. Variability in the response 36
4.2.3. Residual plots 37
4.2.4. Models' summary 40
5. Conclusions 43
5.1. Future work 43
References 45
Annex A: Results of the Principal Stresses of the Specimens 50

List of abbreviations

ABS	Acrylonitrile Butadiene Styrene
AM	Additive Manufacturing
DEGI	Department of Industrial Engineering and Management
DEMec	Department of Mechanical Engineering
DIC	Digital Image Correlation
DLP	Digital Light Processing
ESPI	Electronic Speckle Pattern Interferometry
FDM	Fused Deposition Modelling
FEUP	Faculty of Engineering of the University of Porto
FFF	Fused Filament Fabrication
INEGI	Institute of Science and Innovation in Mechanical and Industrial Engineering
PET	Polyethylene Terephthalate
PETG	Polyethylene Terephthalate Glycol
PLA	Polylactic Acid
SLA	Stereolithography
SLS	Selective Laser Sintering
TRS	Thermal Residual Stresses

List of figures

Figure 1 - Gantt chart of the performed work. 2
Figure 2 - Type I, II and III Residual stresses. 6
Figure 3 - Schematic representation of the Hole Drilling method developed by Soete 8
Figure 4 - Strain Gauge Rosette used to determine residual stresses on the plane, using the Soete method. 8
Figure 5 - Equivalent uniform stresses in the average stress method. 10
Figure 6 - Relations between surface deformations caused by the relaxation of residual stresses, considering hole depth variations. 11
Figure 7 - Residual stress measurement through the Integral Method. 12
Figure 8 - Identical parts made from conventional manufacturing processes (a) vs. Additive manufacturing (b). 13
Figure 9 - Classification of AM technologies. 14
Figure 10 - Steps to produce a part through AM. 14
Figure 11 - Diagram of FFF printing. 15
Figure 12 - Basic principle of Image Correlation 18
Figure 13 - Central Composite Design with three factors 20
Figure 14 - Methodology applied to determine residual stresses in the specimens. 21
Figure 15 - Dimensions of the printed specimen. 23
Figure 16 - Prusa i3 MK3S 3D printer. 23
Figure 17 - Example of a speckle pattern painted on the specimens. 24
Figure 18 - Automatic system for the measurement of residual stresses, MTS3000-Restan... 24
Figure 19 - Drilled hole on printed specimen. 25
Figure 20 - Experimental drilling and image acquisition setup. 26
Figure 21 - Strain gage rosette arrangement for determining residual stresses 27
Figure 22 - Strain gage rosette mounted on printed specimen. 29
Figure 23 - Drilled specimen used for the DIC strain measurement approach. 30
Figure 24 - Principal stresses in Specimen 1a, obtained using strain gage measurement. 30
Figure 25 - Principal stresses in Specimen 1b obtained using DIC measurement. 31
Figure 26 - Principal stresses in Specimen 2a obtained using strain gage measurement. 31
Figure 27 - Principal stresses in Specimen 2b obtained using DIC measurement. 32
Figure 28 - Strain gage rosette formed with virtual extensometers. 33
Figure 29 - Principal stresses in Specimen 1b obtained using DIC measurement with strain averages. 34
Figure 30 - Principal stresses in Specimen 2b obtained using DIC measurement with strain averages. 34
Figure 31 - Pareto chart of the standardized effects on the minimum principal stress. 36
Figure 32 - Pareto chart of the standardized effects on the maximum principal stress. 37

Figure 33 – Residuals versus order plot for minimum principal stress. 38
Figure 34 - Residuals versus order plot for maximum principal stress. 38
Figure 35 - Residuals versus fits plot for minimum residual stress....................................... 38
Figure 36 - Residuals versus fits plot for maximum residual stress. 39
Figure 37 - Normality probability plot of the residuals for minimum principal stress. 39
Figure 38 - Normality probability plot of the residuals for maximum principal stress. 39
Figure 39 - Contour plot of minimum residual stress vs. feed rate and extrusion temperature. 41
Figure 40 - Contour plot of maximum residual stress vs. feed rate and extrusion temperature 41
Figure 41 - Principal Stresses measured in Specimen 3 50
Figure 42 - Principal Stresses measured in Specimen 4 50
Figure 43 - Principal Stresses measured in Specimen 5 51
Figure 44 - Principal Stresses measured in Specimen 6 51
Figure 45 - Principal Stresses measured in Specimen 7 52
Figure 46 - Principal Stresses measured in Specimen 8 52
Figure 47 - Principal Stresses measured in Specimen 9 52
Figure 48 - Principal Stresses measured in Specimen 10 53
Figure 49 - Principal Stresses measured in Specimen 11 53
Figure 50 - Principal Stresses measured in Specimen 12 53
Figure 51 - Principal Stresses measured in Specimen 13 54
Figure 52 - Principal Stresses measured in Specimen 14 54
Figure 53 - Principal Stresses measured in Specimen 15 54
Figure 54 - Principal Stresses measured in Specimen 16 55
Figure 55 - Principal Stresses measured in Specimen 17 55
Figure 56 - Principal Stresses measured in Specimen 18 55
Figure 57 - Principal Stresses measured in Specimen 19 56
Figure 58 - Principal Stresses measured in Specimen 20 56

List of Tables

Table 1 - Properties of PETG . 16

Table 2 - Design of Experiments created to determine the influence of printing parameters in residual stresses. 21

Table 3 - Varying factors in the Design of Experiments. 22

Table 4 - Constant printing parameters. 22

Table 5 - Equivalent principal plane stress of each specimen. 32

Table 6 - Analysis of variance of the minimum principal stress. 35

Table 7 - Analysis of variance of the maximum principal stress. 35

Table 8 - Model summary for the minimum principal stress response. 40

Table 9 - Model summary for the maximum principal stress response. 40

Table 10 - Paremeter values which minimize the formation of residual stresses. 42

1. Introduction

The present report was written within the scope of the Dissertation project aimed at concluding the master's degree in mechanical engineering at the Faculty of Engineering of the University of Porto (FEUP). It focuses on studying the influence of printing parameters on the formation of residual stresses on additively manufactured parts. The work developed was carried out at the "Instituto de Ciência e Inovação em Engenharia Mecânica e Engenharia Industrial" (INEGI) between February and June of 2023.

1.1. Project motivation

Additive manufacturing is a process that has been gaining increased relevance in the industry. However, one of the disadvantages of this manufacturing process is the occurrence of the phenomenon of residual stresses, associated with temperature gradients and varying cooling rates inherent to the process. Thus, it's important to understand how the different printing parameters affect the appearance of these stresses in the manufactured parts in order to reduce their negative influence and optimize their mechanical properties.

INEGI, as a technology interface centre, specializes in carrying out research and innovation activities based on technology. This, coupled with its close working relationship with FEUP, make it an ideal place to develop this research project.

1.2. Host institution

INEGI is a non-profit institution that promotes the interface between Industry and University, helping the transfer of technology and technological innovation aimed at economic development. It was founded in 1986 within what are now the Departments of Mechanical Engineering (DEMec) and Industrial Engineering and Management (DEGI) at FEUP.

As a Private Non-Profit Association with the status of "Public Utility" and its own team of over 275 collaborators, it assumes an active role in the development and consolidation of a competitive model based on knowledge, technological density of products and processes, and technological innovation.

INEGI's mission is to contribute to the increase of the national industry's competitiveness through research and development, demonstration, technology transfer, and training in the areas of design and project, materials, production, energy, maintenance, industrial management, and environment. Its goal is to be a national reference institution and a relevant element of the European scientific and technological scope, with merit and excellence in technological innovation and knowledge transfer.

Currently, INEGI has 134 researchers and over 135 innovation projects in the industry, being the largest R&D, Innovation and Technology Transfer unit in Mechanical Engineering in Portugal. It has a working relationship with 736 entities, including the university, business associations, public entities, as well as 398 international partners.

The institution has a very comprehensive set of resources to support its activities, including laboratories for experimental work, workshops for component development and pre-series, and a vast set of computer tools to support engineering work.

1.3. Project objectives

The primary focus of this project is to conduct an in-depth investigation into how different printing parameters affect the presence and magnitude of residual stresses in 3D printed specimens. The chosen printing parameters were layer height, extrusion temperature and feed rate.

Additionally, the project will introduce virtual extensometers as a non-contact measurement technique for quantifying residual stresses. The virtual extensometers will utilize digital image correlation (DIC) to calculate strains directly from images captured during mechanical testing.

1.4. Project planning

The project was divided into six phases. Firstly, an extensive literature review was conducted to gather existing knowledge on the subjects addressed. Secondly, a detailed plan was developed for the design of experiments, specifying variables, parameters, and procedures. The third phase involved manufacturing specimens according to the experiment design. Subsequently, mechanical tests were conducted on the specimens to evaluate the residual stresses. The fifth phase focused on analysing the results obtained, identifying patterns, and engaging in discussions related to the findings. Lastly, a comprehensive dissertation report was written, summarizing the research process, methodology, results, and interpretations.

The duration of each phase is presented in the Gantt chart in figure 1.

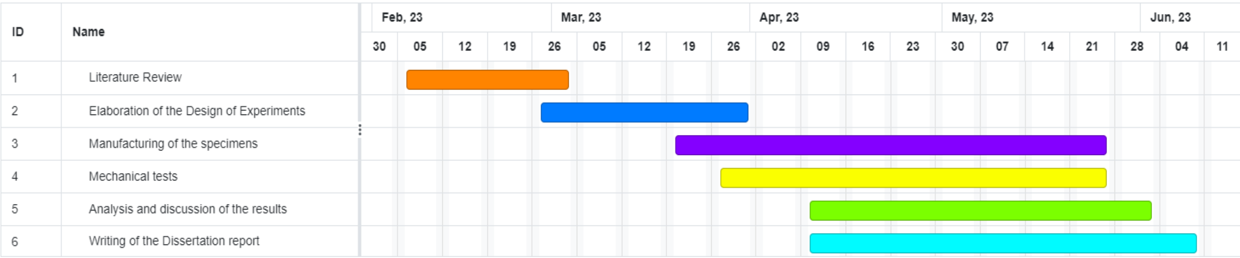

Figure 1 - Gantt chart of the performed work.

1.5. Dissertation structure

The upcoming chapters of the dissertation will encompass the following: Chapter 2 will entail a literature review, presenting existing knowledge and research relevant to the topic. Chapter 3 will delve into the methodology, providing a detailed description of the research design, data collection, and analysis techniques employed in the study. Finally, Chapter 4 will serve as the conclusion and future work section, summarizing the key findings, discussing their implications, and suggesting potential areas for future research and development.

2. Literature review

2.1. Residual stresses

Residual stresses can be defined as those that remain in a material or component after the manufacturing process and in the absence of external forces or thermal gradients (James and Lu, 1996). Manufacturing processes are the most common cause of residual stresses, as virtually all of them (casting, welding, machining, additive manufacturing, among others.) introduce residual stresses in the manufactured components. However, they can also arise from maintenance or repair operations. Sometimes, these stresses can also be induced in service, during the installation process or by occasional overloads.

Residual stresses can be classified into macro or micro stresses, and either type, in combination or individually, may appear in a component. Macro residual stresses, often referred to as Type I residual stresses, vary along the component on a much larger scale than the grain size. Micro stresses, resulting from differences in the material's microstructure, can be classified as Type II or III. Type II residual stresses are micro stresses that operate at the grain size level, and Type III stresses are generated at the atomic level (James and Lu, 1996).

The effects of residual stresses can be both beneficial and detrimental, depending on their magnitude, sign, and distribution. In most cases, residual stresses are detrimental, as they overlap with service stresses. There is a lot of documentation on cases where these stresses are considered the predominant factor in structural failures. An example of the effect of residual stresses and material properties on the behaviour of structures can be found in the work done by Piloto et al (2002) on the behaviour of structures under fire action. However, they can also be beneficial, especially by allowing the increase of the fatigue limit stress in dynamically loaded components. In these cases, compressive residual stresses are intentionally induced on the surface, such as in shot peening (Nobre, 2000), applied on surfaces, and cold work (Papanikos, 1997), applied in rivet holes. Both techniques are widely used in aircraft construction. Another particularly important aspect of residual stresses is that their presence generally goes unnoticed until malfunction or failures occur (Ribeiro, 2006).

There are currently different techniques for measuring residual stresses, such as layer removal and curvature, X-ray and neutron diffraction, magnetic and ultrasonic techniques, among others. The hole-drilling method with extensometry or with optical processes in which radiation is in the visible range are the ones focused on in this study. Some of them use mechanical stress relief processes to be able to measure them, while in others their presence is detected by the effects on the material properties. However, none of them are generally applicable and allow easy use. Therefore, the need to investigate new techniques and applications that allow the characterization of residual stress fields is justified.

Given the importance of this topic, it was decided to develop a research project that would allow for the adaptation of optical techniques to measure residual stresses using the hole-drilling method, more specifically, the Digital Image Correlation (DIC) technique.

The use of the hole-drilling method involves the use of experimental techniques to obtain surface deformations caused by the release of stresses. These deformations can be measured using discrete measurement transducers or calculated from surface displacements. Optical techniques used for displacement measurement offer significant advantages compared to other techniques, including the ability to perform global or field measurements, perform contactless measurements on and off the plane, and the ability to vary resolution from low (tenths of a millimetre) to very high (a few tenths of a micrometre), depending on the lighting (Ribeiro, 2006).

As these techniques rely on comparing two states of a surface (before and after deformation), it is always necessary to create different reference patterns depending on the technique used, which can be classified into two groups: random patterns and regular patterns (lines and grids). Random patterns allow for displacement measurement in different directions. These patterns can be artificially created on uniform surfaces by applying droplets of ink to the surface using spray painting for example. Granulated inks available in the market can also be used, or the natural microscopic roughness of the surface can be used as a random reference pattern. The image correlation technique is used for the first case, but this technique can only be used for displacement measurement when the required resolution is not very high since the dimensions of these patterns are quite large compared to the wavelength of light. The second case allows for measurement with high resolution, but it is always necessary to use coherent light illumination, such as laser light. One of the optical techniques that uses this type of reference is Electronic Speckle Pattern Interferometry (ESPI). The former approach was selected for this study due to its simpler experimental setup and equipment requirements.

In this work, a technique was developed to congregate the hole-drilling method with digital image correlation in order to determine residual stresses in specimens based on the displacements on the speckle pattern onto the printed specimens.

2.2. Influence of Residual Stresses on components

With the use of current analytical and computational approaches, it is frequently possible to estimate the stresses that a component is subjected to over the course of its life. However, this is insufficient to evaluate the part's performance over the course of its service life. The residual stresses that might exist in the examined component must be considered for a more accurate outlook (Withers, 2001).

According to Withers (2001), residual stress is the stress that remains in a body that is stationary when all applied stresses have been removed. It is of great relevance to be able to define and quantify these stresses as they, combined with applied stresses, can cause failure at levels below that at which failure would occur from applied stresses alone.

Even though residual stresses determination is crucial, estimating them is challenging since, unlike applied stresses, they cannot be computed from the forces and impulses that a material, component, or assembly experiences.

Residual stresses can be classified into different categories depending on their origin (such as thermal mismatch stresses), the measurement method (such as destructive, semi-destructive, or non-destructive), or the scale over which they self-equilibrate (e.g., macro- or micro-stresses).

Residual stresses can be accommodated over relatively short distances, known as micro stresses, or they might span larger distances, known as macro stresses. Materials can be inhomogeneous both on the atomic scale as well as on larger scales. Examples of this include pores, inclusions, segregated grains, reinforcing fibres or particles, dislocations, precipitates, or isolated grains. These irregularities cause the stress field to be disturbed. Because of this, measured stress may be reported as uniform over wider areas but becomes significantly nonuniform when the sample area gets closer to the size of the inhomogeneities (Braga and Castro, 2012).

Since residual stresses by definition exist in the absence of external loading, equation 2.1 states that they must balance to zero within a restricted volume.

$$\int_V \sigma_{Res} dV = 0 \tag{2.1}$$

A characteristic length that can be utilized to distinguish between macro stresses and micro stresses is defined by the dimensions of the smallest volume V across which the residual stresses will balance. The characteristic length of macro stresses is on the order of the component's dimensions as they balance to zero when integrated over the cross section of the component. The material can therefore be regarded as homogeneous in the case of macro stresses (Braga and Castro, 2012).

Residual micro stresses are those that exist between grains in polycrystalline materials, between phases in multiphase materials (for example, between the matrix and reinforcement in composites), or around other microstructural features including dislocations or precipitates as a result of the presence of inhomogeneities on a smaller scale. The local changes in stress from the macro stress value within the material's inhomogeneities are subsequently referred to as micro stresses. Thus, over a characteristic length of the order of the microstructural features causing them, micro stresses will balance to zero (Johnson, 2008).

The impact of macro stresses is more significant for general engineering purposes since they have a discernible impact on the total loads placed on solids or structures. Micro stresses can also have significant local impacts, such as in surface treatment.

Type I, II, and III are often used classifications to characterize residual stresses. Residual macro stresses, or Type I, are those that balance themselves over a considerable length (considering 1-D stress for convenience). Residual micro stresses of Type II balance on a scale according to grain size. Although Type III residual micro stresses also result from point and dislocation flaws inside grains, they balance to zero over a characteristic length that is less than the grain dimensions (Johnson, 2008). These three types of residual stresses are schematically pictured in figure 2.

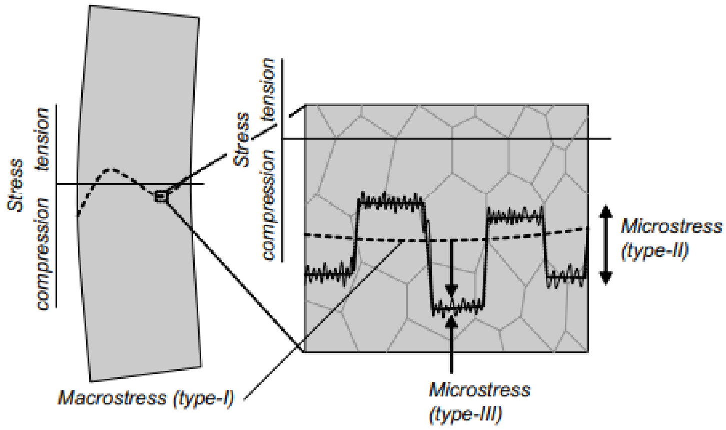

Figure 2 - Type I, II and III Residual stresses (Johnson, 2008).

One of the failure stages that is greatly influenced by residual stress is cracking. The amplitude and sign (compressive or tensile) of the residual stress, as well as the cyclic deformation behaviour of the structural region of interest, determine the influence of residual stress on fatigue-crack initiation life (Johnson, 2008).

Residual stress can increase or decrease the fracture propagation time when a component is subjected to cyclic loads and the local stress-strain response is linear-elastic. Tensile residual stress shortens the fatigue life of a crack. On the other hand, the fatigue life is lengthened if a crack is located in a region that is susceptible to compressive residual stress.

Compression/tensile residual stresses also influence retardation/acceleration impact. The expanding fatigue fracture will produce its own residual stress field, both before and after the tip, according to this reference. Crack closure, a process that slows the formation of cracks, is caused when compressive residual stress is left behind after the tip of a fatigue fracture (Johnson, 2008).

The R-ratio, or minimum to maximum stress ratio, is typically used to describe mean stress. S-N (stress-life) curves for the target material, geometry, and surface finish can be used in conjunction with well-known constant-life models to quantify the impact of R-ratio on high-cycle fatigue behaviour. This stress-based assessment method is frequently used on rotating machinery, welded components, pressure vessels, and aircraft structures subjected to alternating loads (Johnson, 2008).

The Influence of residual stresses on stable cyclic fatigue depends on numerous variables, including crack size, mechanical load variables, crack closure effects, and the environment. These all affect the formation of cracks in engineering materials. The stress intensity factor range, $\Delta K = (K_{max} - K_{min})$ of the load cycle, can be used to describe the growth rate per cycle (da/dN) of lengthy cracks. A plot of $log(da/dN)$ vs $log(\Delta K)$ for several engineering materials shows a sigmoidal variation with three regions: a threshold regime, an intermediate Paris-Law regime, and a high growth rate regime. The load R-ratio ($R = K_{min}/K_{max}$) is increased by tensile residual stresses in the fracture location, which accelerates crack propagation in all three behaviour regimes.

It is well known that tensile residual stresses have a negative impact on fatigue life, as well as on stress corrosion and fracture development in materials. Contrarily, compression stresses can be advantageous in certain areas by preventing the initiation and propagation of cracks. Technological processes, such as quenching, welding, casting, or additive manufacturing, may unintentionally generate residual stress. On the other hand, shot peening can be used to deliberately induce compressive stresses, increasing fatigue resistance (Neto et al, 2022).

Significant increases in fatigue life may result from slower fatigue crack growth (FCG), according to Lacarac et al, (2000). A component's fatigue behaviour improvement is usually attributed to:

- Increases in the yield stress of the material by the strain hardening of surface layers,
- The compressive residual stresses in surface layers,
- The final surface finish quality and structural changes.

The emergence of distinct forms of crack growth (i.e., with and without crack closure) can be attributed to the redistribution of residual stresses as a result of crack propagation (Neto et al, 2022).

Neto et al. (2022) also studied the effects of residual stresses on fatigue crack growth and it was determined that elastic thermal residual stresses (TRS) are distributed differently as a result of fatigue crack propagation. The TRS is increased by the residual stresses brought on by the plastic deformation of the fracture tip. Apart from this, the regions with tensile TRS show an increase in *da/dN*, while the regions with compressive TRS show a decrease in *da/dN*. A perfect match exists between the trends of *da/dN* and the original profile of TRS.

Considering this, it’s important to minimize the negative aspects of residual stresses introduced by different manufacturing methods, and in the context of this project, particularly additive manufacturing of PETG. This can be done by tuning the printing parameters in order to maximize the mechanical properties of the final component and minimize the presence of tensile residual stresses.

2.3. Hole Drilling method

Since the 1930s, residual stresses have been measured using perforations. Mathar (1934) developed a technique for computing uniaxial residual stresses that entailed monitoring changes in the dimension of a hole that had been cut out of a specimen. Soete used electric strain gauges, which were developed in 1937, to track surface deformations generated by residual stresses released around a drilled hole (Soete, 1950). Because the residual stress field is viewed as being uniform throughout the entire thickness of an infinite isotropic plate, this method enables the use of Kirsch's solution (Kirsch, 1898).

The relaxation of residual stresses results in the strain recorded on a strain gauge in the radial direction for a residual stress field with known major directions. When a small through-hole is made to achieve this relaxation, the radial strain can be noted as follows:

$$\varepsilon_r = \frac{1}{E}\frac{2r_0}{r_1 r_2} cos2\theta \left[-1 + \frac{1+\nu}{4}\frac{{r_0}^2({r_1}^2 + r_1 r_2 + {r_2}^2)}{{r_1}^2{r_2}^2}\right](\sigma_1 - \sigma_2) - \frac{(1+\nu){r_0}^2}{2E r_1 r_2}(\sigma_1 + \sigma_2) \quad (2.2)$$

Where r_0 is the radius of the hole and r_1 and r_2 are the radial coordinates of the extremities of the electric strain gauge and $\varepsilon_m = \frac{1}{r_1 - r_2}\int_{r_1}^{r_2} \varepsilon_r \, dr$ is the value for equivalent deformation in the situation depicted in figure 3.

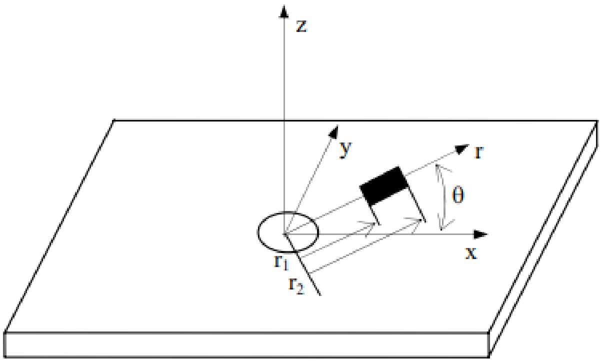

Figure 3 - Schematic representation of the Hole Drilling method developed by Soete (Ribeiro, 2006).

Equation 2.1 can be rewritten as:

$$\varepsilon_m = A(\sigma_1 + \sigma_2) + B(\sigma_1 - \sigma_2)\cos 2\theta \qquad (2.3)$$

Where A and B are coefficients which can be calculated through the following expressions:

$$A = -\frac{1+\nu}{2E}\frac{{r_0}^2}{r_1 r_2} \qquad B = \frac{1}{E}\frac{2{r_0}^2}{r_1 r_2}\left[-1 + \frac{1+\nu}{4}\frac{{r_0}^2({r_1}^2 + r_1 r_2 + {r_2}^2)}{{r_1}^2 {r_2}^2}\right]$$

The primary residual stresses σ_1 and σ_2 can be identified from de radial deformations in directions θ_1 and θ_2 in equation 2.3, where r_0, r_1 , r_2, E and ν are defined. The three components of residual stress, σ_{xx}, σ_{yy} and τ_{xy}, must be determined using three extensometers placed over the circumference of radius r_m with different directions if the principal directions are unknown, as shown in figure 4.

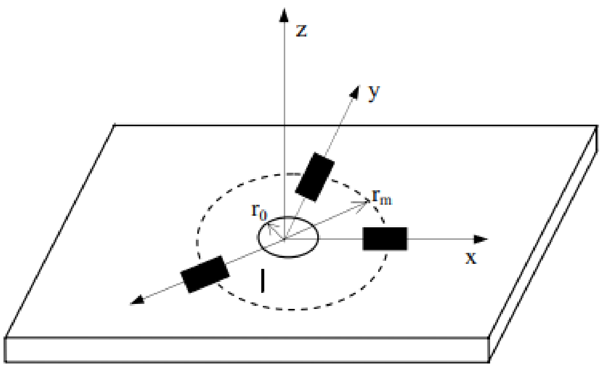

Figure 4 - Strain Gauge Rosette used to determine residual stresses on the plane, using the Soete method (Ribeiro, 2006).

The through-hole approach comes with several built-in limitations. First of all, it assumes that residual stresses are self-equilibrating. For this condition to be held, the stress distribution must be uniform over the thickness of the plate. Secondly, a through hole can render a structure or component useless in some applications where residual stresses need to be measured.

Nevertheless, a measurement using the through hole approach does not produce additional meaningful data, as residual stresses are present in the surface layers.

When residual stresses are distributed unevenly over the thickness, Soete and Vancombrugge's (1950) incremental deformation approach enables the determination of residual stresses. This methodology was created to make strain gauge measurements compatible with the blind hole method. Since they vary with thickness, the coefficients A and B in equation 2.3 are treated as calibration constants in this method (Ribeiro, 2006).

Theoretically, the average residual stress in an incremental layer is proportional to the change in deformation at the surface of a hole drilled in incremental fashion. This suggests that if the mean stress along a depth increment is the same for the uniform and non-uniform stress states, the surface deformation in both conditions should be identical. Using Hooke's law, incremental deformation could be calculated, according to Kelsey (1956), by accounting for:

$$\Delta\varepsilon_{xx} = \frac{1}{E}(K_1^i\sigma_{xx} - \nu K_2^i\sigma_{yy}) \qquad \Delta\varepsilon_{yy} = \frac{1}{E}(K_1^i\sigma_{yy} - \nu K_2^i\sigma_{xx}) \qquad (2.4)$$

The average residual stresses along the thickness of the hole may be determined through equations 2.4, resulting in:

$$\sigma_{xx} = \frac{E}{(K_1^i)^2 - (K_2^i)^2}\left[K_1^i(\Delta\varepsilon_{xx}) + \nu K_2^i(\Delta\varepsilon_{yy})\right]$$

$$(2.5)$$

$$\sigma_{yy} = \frac{E}{(K_1^i)^2 - (K_2^i)^2}\left[K_1^i(\Delta\varepsilon_{yy}) + \nu K_2^i(\Delta\varepsilon_{xx})\right]$$

The coefficients K_1^i and K_2^i are derived numerically or through experimental calibration. The component where residual stresses are to be measured's material should match that of the calibration specimen. For this, a strain gauge rosette is applied to the calibration specimen's surface and used to quantify surface deformations. Hole drilling and deformation measurement are done according to traditional practices.

Every measurement that is made using the Kelsey method needs to be previously calibrated. To characterize the change of surface deformation with hole depth, Rendler and Vigness (1966) presented a function. The variation in deformation when drilling is increased from a depth of z to z + Δz is as follows:

$$\Delta\varepsilon(\varphi) = [K_z(\varphi)\sigma_z\Delta \mathrm{z}] \qquad (2.6)$$

Where σ_z represents the residual stress for a depth of z, φ is the angle between the direction of the measurement and the maximum principal direction, $\Delta\varepsilon(\varphi)$ is the radial deformation for a certain radial distance caused by the drilling of a depth Δz. $K_z(\varphi)$ is a parameter which is constant for any given z, Δz and φ. To simplify, it may be considered that z corresponds to the total depth of the hole, and in this case equation 2.6 can be rewritten as:

$$\varepsilon(\varphi) = [K(\varphi)]\sigma, \text{ and } K(\varphi) = A + B\cos 2\varphi \tag{2.7}$$

Where A and B are coefficients which can be expressed by:

$$A = \frac{1}{2E}(k_1 - \nu k_2) \qquad B = \frac{1}{2E}(k_1 + \nu k_2)$$

Where k_1 and k_2 are constants for isotropic materials. Consequently, for isotropic materials, calibration is only required once.

Incremental calibration approaches include those developed by Kelsey and Rendler as well as other researchers during this time. The method of average stresses is a different approximation technique that was developed by Nickola (1986). The idea of equivalent uniform stress was created for this method. It is the uniform stress that would be present throughout the entire depth of the hole and would result in the same relaxation of deformation as the actual non-uniform stress distribution. The following equation can be used to determine the change in stress brought on by a new increase in hole depth:

$$\Delta\sigma_n = \frac{1}{\Delta h_n}[\sigma_n h_n - \sigma_{n-1} h_{n-1}] \tag{2.8}$$

Where $\Delta h_n = h_n - h_{n-1}$; σ_n and σ_{n-1} are the equivalent uniform stresses at hole depths h_n and h_{n-1}, as can be seen in figure 5.

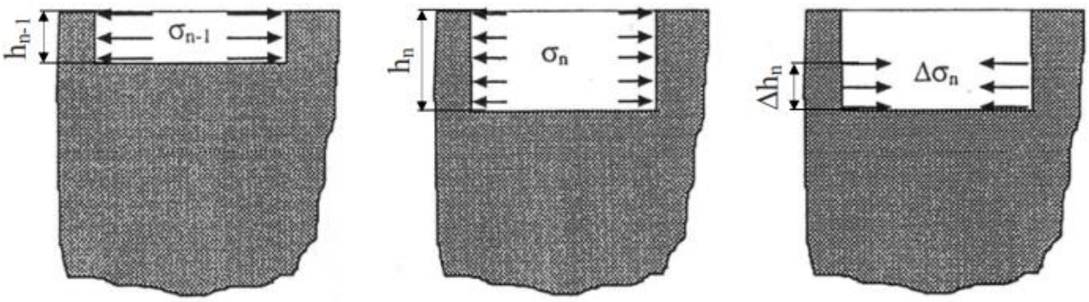

Figure 5 - Equivalent uniform stresses in the average stress method (Ribeiro, 2006).

Since the surface deformation around a blind hole caused by the relaxation of non-uniform stresses in depth may not be equivalent to the deformation caused by externally applied loads, experimental calibrations for the incremental deformation method and the average stress method can be very time-consuming, and it becomes very challenging to prepare calibration specimens with the appropriate residual stresses. When residual stress varies with depth, the computed stresses using these methods at intermediate depths don't represent the actual residual stress. Instead, they represent the equivalent uniform stress (from the surface to depth h) that would result in the same relaxation of deformation at that depth. Schajer (1981) makes reference to this circumstance, which is schematically depicted in Figure 6.

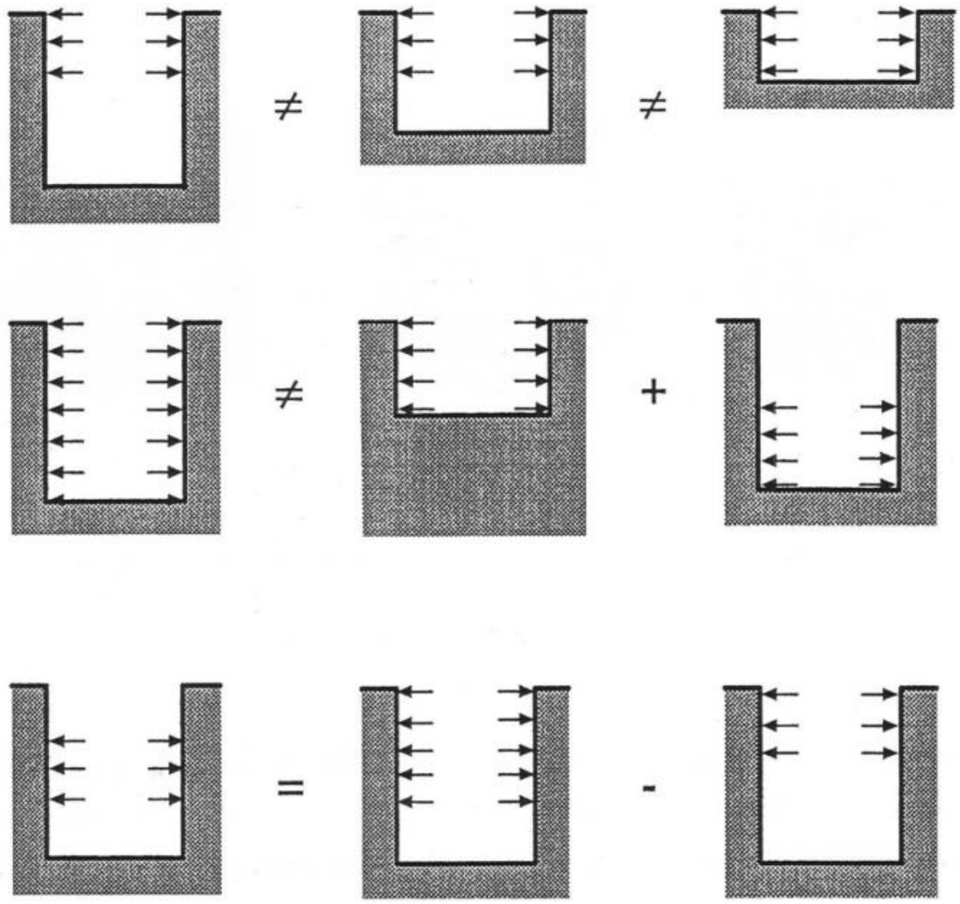

Figure 6 - Relations between surface deformations caused by the relaxation of residual stresses, considering hole depth variations (Ribeiro, 2006).

In conjunction with the advancement of the finite element method, Schajer (1981) introduced a numerical calibrating method. This technique simulates the relaxation of residual stresses by applying external loads to the hole's edge. A calibration specimen with all conceivable geometrical shapes and dimensions can be used to derive the calibration coefficients A and B in equation 2.2. The shortcomings of the incremental deformation and average stress methods were then overcome by the development of the integral method by Bijak-Zochowski (1978), Niku-Lari (1985), Lu (1986), Flaman (1985), and Schajer (1988) for situations with non-uniform residual stresses. The stresses are considered to be uniform over a limited depth of the hole, which corresponds to the depth of each increment, in the integral method, as can be seen in Figure 7 (Ribeiro, 2006).

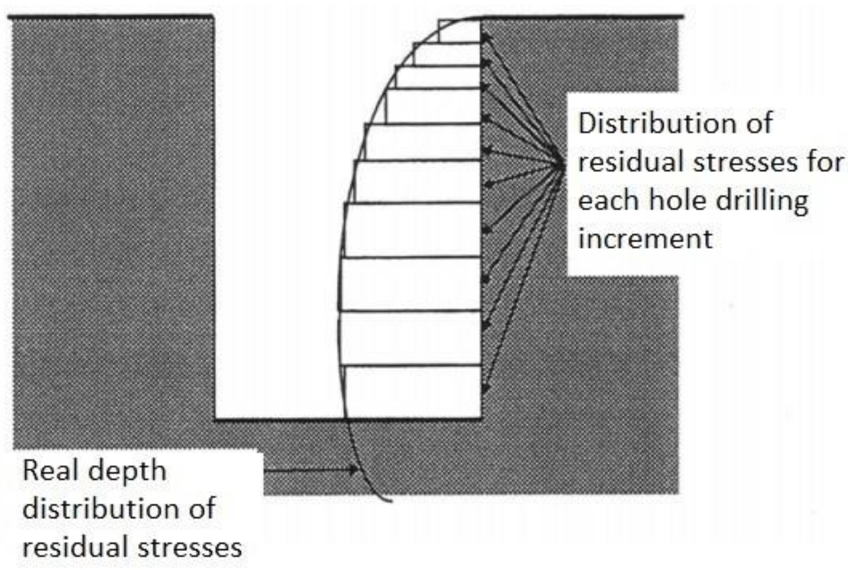

Figure 7 - Residual stress measurement through the Integral Method (Ribeiro, 2006).

The relationship between the deformation caused by the uniform residual stresses present across the surface during each drilling step and the corresponding residual stresses can be expressed through equation 2.3. However, in this case, the calibration coefficients are different. Thus, the referred equation may be expressed in the matrix form as follows:

$$\varepsilon_r{}^i = \sum_{j=1}^{i} \left[A^{ij} + B^{ij}\cos 2\theta \;\; A^{ij} - B^{ij}\cos 2\theta \;\; 2B^{ij}\sin 2\theta \right] \begin{bmatrix} \sigma_{xx}^j \\ \sigma_{yy}^j \\ \tau_{xy}^j \end{bmatrix} \qquad (2.9)$$

Where $i = 1,2,\dots,n$; n is the total number of increments; $j = 1,2,\dots,i$; A^{ij}, B^{ij} are calibration coefficients of the layer j, after the completion of increment i; σ_{xx}^j, σ_{yy}^j, τ_{xy}^j are the residual stress components of layer j.

The integral method has proven to be more precise than other hole drilling techniques for measuring non-uniform residual stresses, especially when those stresses vary abruptly over the thickness. (Ribeiro, 2006).

In many technical applications currently, methods based on stress relaxation with a drilled hole and strain gauge measurement and particularly the integral method, are considered to be trusted methods. In literature, a wide range of applications have been addressed, including situations involving heat treatments, surface treatments, machining, welding, and surface coatings of composite materials. This includes the study of heat treatments on the presence of residual stresses of TI-6AL-4V parts produced by additive manufacturing (Teixeira et al, 2020) and the study of welding residual stresses and their effects on fracture in pressure vessels and piping components (Dong and Brust, 2000).

2.4. Additive manufacturing

In contrast to subtractive manufacturing and formative manufacturing approaches, additive manufacturing (AM) is defined in international regulations as "the process of combining materials to make components from data from 3D models, usually layer upon layer" (Slotwinski, 2021). AM methods are unique from other manufacturing techniques since they are driven by digital designs and produce things one layer at a time. Figure 8 shows how additive manufacturing differs from conventional production techniques (Slotwinski, 2021).

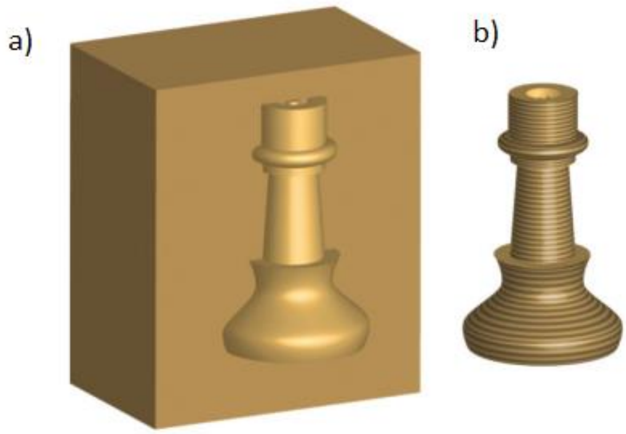

Figure 8 - Identical parts made from conventional manufacturing processes (a) vs. Additive manufacturing (b) (Slotwinski, 2021).

Compared to traditional methods of material removal and forming, AM has a number of benefits. Among them are the abilities to:

- Create components with incredibly intricate geometry (including internal features),
- Simplify mass customization to make it easy to make particular part alterations, including those that allow biomedical implants to account for each patient's geometry,
- Create parts from hard-to-machine materials (like tungsten or titanium),
- Combine several part assemblies into a single monolithic part,
- Create parts with purposefully induced surface porosity, which improves the functionality of biomedical implants by providing structures for osseointegration,
- Quickly speed up new part development and prototyping, even in situations where AM is not the best option.

AM technologies are divided into various classes, each with a unique set of capabilities, materials, system costs, infrastructure requirements, and skill levels needed to make parts (Slotwinski, 2021). The many AM method classifications are displayed in Figure 9.

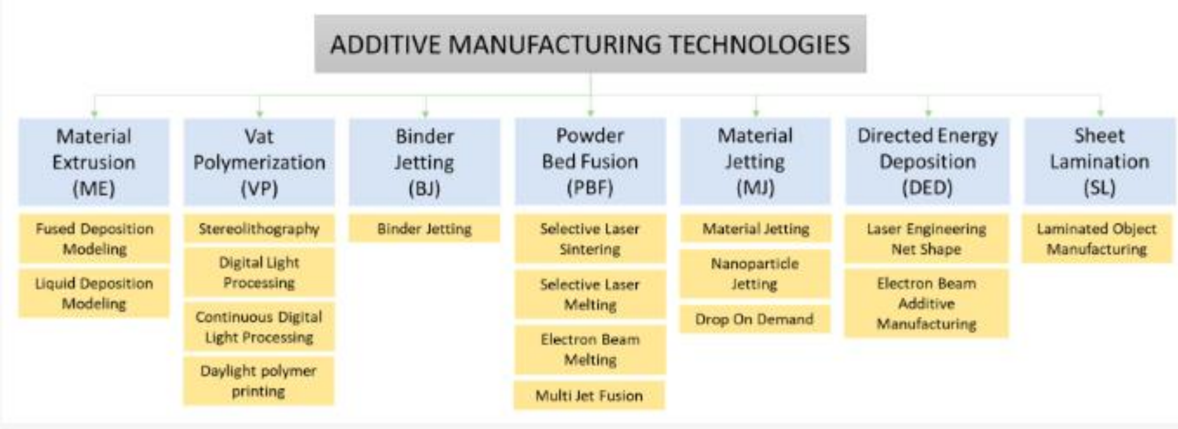

Figure 9 - Classification of AM technologies. (Mohan et al, 2020)

Figure 10 depicts a summary of the steps that need to be taken from the part design to its manufacturing using 3D printing. To create a 3D printed part, the process typically involves the following steps. First, a 3D design of the part is created using specialized software, specifying its shape and details. This design is then converted into an STL file format, which represents the geometry of the 3D model. The next step involves using slicing software to convert the design into G-code instructions, which determine the printing parameters and tool paths. Finally, the 3D printer is prepared, and the G-code file is transferred to the printer. The printer follows the instructions layer by layer, depositing or curing the material to create the physical object based on the design specifications.

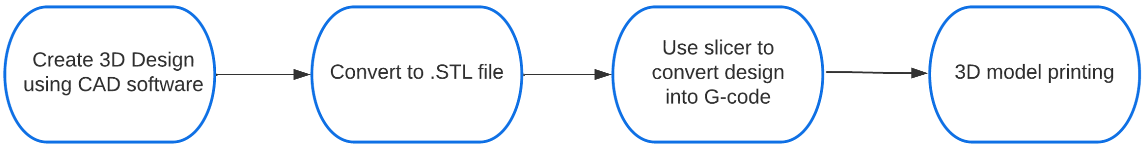

Figure 10 - Steps to produce a part through AM.

While Fused Filament Fabrication is the most widely adopted additive manufacturing method, there are alternative methods worth considering. These include methods such as Selective Laser Sintering (SLS), Stereolithography (SLA), and Digital Light Processing (DLP). SLS employs a laser to sinter powdered polymer materials, creating solid objects layer by layer. SLA and DLP use photopolymerization, where liquid resin is selectively cured by light to form the desired shape. Each of these methods offers distinct features, such as high resolution, greater design freedom, or the ability to print with a wider range of materials (Slotwinski, 2021). However, for the purposes of this study, FFF was chosen due to its wide adoption, accessibility, and suitability for the research objectives in polymer printing.

2.4.1. Fused Filament Fabrication

Fused Filament Fabrication (FFF), also known as Fused Deposition Modelling (FDM), which uses a spool of thermoplastic filament as feedstock, is now the most popular and affordable additive manufacturing technique. The thermoplastic filament is melted in a liquefier and extruded onto the construction platform using predefined tool paths during this process. The process is repeated several times until each layer is complete, and the following layer is then placed on top of the preceding one. Up until the completion of the entire section, the process is repeated. The layer-by-layer method has the potential to produce three-dimensional complex components at low cost and with great efficiency while allowing for design freedom. A schematic illustration of the FFF printing procedure is shown in Figure 11 (Gao et al, 2020).

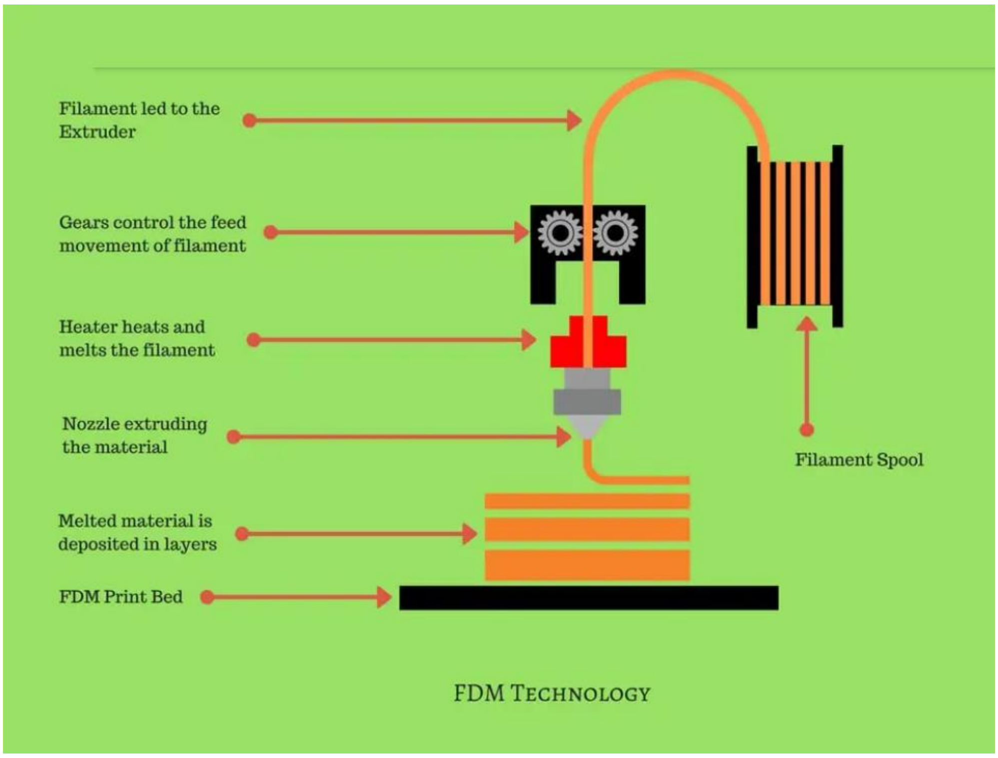

Figure 11 - Diagram of FFF printing. (Manufactur3d, 2018)

FFF also has the benefit of enabling the deposition of many materials, enabling the printing of parts with different functions and/or colours. FFF has so far been widely applied in a variety of fields, including daily life, tissue engineering, the automotive industry, and the aerospace industry. Many parts produced by this method have complex geometries, making their development and production using traditional subtractive manufacturing techniques time and money consuming. FFF is ideal for creating these complicated components without the use of tooling or moulds since it deposits materials at specific locations within each layer. This effectively cuts down on the time and expense needed for the design and production of new parts (Gao et al, 2020).

One major drawback is the relatively slow production speed compared to traditional methods. Additionally, materials used in additive manufacturing may lack the same strength and durability as those in conventional manufacturing, affecting the quality and reliability of printed parts. High initial setup costs and limited standardization further hinder its widespread adoption. However, ongoing research and advancements are addressing these challenges, making additive manufacturing a promising technology for the future.

The wide user access to FFF technology contributed to its choice over other AM processes to be used in this study, since minimizing the negative influence of residual stresses on parts produced by this technique would contribute to the improvement of the quality and reliability, thus making it increasingly appealing to consumers. (Wong, 2012)

2.4.2. Material

One of the most produced and used thermoplastics worldwide is PET, a semi-crystalline polymer. Among other things, PET is used to make disposable plastic bottles, flexible packaging for food, electronics, and some fabrics. The glass transition temperature (T_g) of PET is approximately 67°C, making it an appealing engineering plastic and its tensile strength is in the 50 MPa range (Holcomb et al, 2022).

A major PET copolymer that is frequently used in AM, poly(ethylene terephthalate) glycol (PETG), has a higher T_g yet is mechanically comparable to PET. PETG, on the other hand, has a lower melting point and viscosity than PET. Its amorphous form is brought about by the glycol group. Due to these characteristics, PETG is a more advantageous polymer for FFF applications. PETG is frequently regarded as an adequate intermediate 3D printing filament between ABS and PLA (Holcomb et al, 2022).

Both ABS (acrylonitrile butadiene styrene) and PLA (polylactic acid) are popular materials used in AM. ABS is a thermoplastic polymer known for its strength, durability, and impact resistance. Meanwhile, PLA is a biodegradable and environmentally friendly thermoplastic widely used due to its ease of printing, low toxicity, and availability in various colors.

PETG can bridge the gap between PLA and ABS in AM since its filament shape yields sturdy prints with little to no warping and no hazardous emissions. Additionally, PETG exhibits better elongation at break than PLA and is less brittle and comparatively heat resistant. However, PETG has some drawbacks of its own, such as a propensity to string and ooze when printed (Holcomb et al, 2022).

PETG is additionally renowned for being highly chemically resistant, biocompatible, transparent, and recyclable. It has a suitable flammability rating and can be utilized in a variety of indoor applications, including those involving food, medicine, and electronics. It is less effective against scratching and frictional contact, has poor ultraviolet light resistance, and also poor scratch resistance (Guessasma, 2019). Table 1 below shows some mechanical and thermal characteristics of PETG.

Table 1 - Properties of PETG (Ansys, 2022).

Property	Value
Young’s modulus	2.01-2.11 GPa
Poisson’s ratio	0.395-0.411
Yield Strength	47.9-52.9 MPa
Melting Point	209-249 ºC
Glass temperature	81-91 ºC

Thermal expansion coefficient	120-123 με/ºC

2.5. Digital Image Correlation

Optical methods can be used for determining displacements in the plane. These techniques compare the component's undeformed and deformed states to produce the results. It is required to establish reference points that allow for the characterization of the deformation or movement of the surface of the structure or component under testing in order to enable this comparison. These references may be etched into the surface or come from the texture of the component itself. Grids of parallel lines, grids of intersecting lines, and grids of points are the three different forms of references that can be made on the surface of a part. (Ribeiro, 2006) For this work, a grid of randomly distributed points, referred to as speckle pattern was used to determine the deformations on the surface of the specimens in analysis.

The application of random patterns on the surface of components or structures is the foundation of digital image correlation (DIC). The method is based on the analysis of two photographs taken in distinct states—one prior to deformation (reference image) and the other following deformation (deformed image) (Ribeiro, 2006).

This measurement method calculates displacements on surfaces of parts or structures exposed to thermal or mechanical loads using a mathematical correlation method. This method makes use of multiple photos taken in succession while the component is subject to loads. The displacements that occurred are then calculated using pairwise correlation between these images (Ribeiro, 2006).

The random pattern on the surface of the component is later subdivided into smaller areas, whilst DIC processing takes place. Following that, each subdivision identified in the initial image will be compared using correlation to images collected for the object's various stages of deformation, $f(x, y)$ and $f^*(x^*, y^*)$. By using the image's real dimensions, it is possible to calculate the average relative displacement of each image subdivision (Chu, 1985).

The image correlation process is depicted in its most basic form in Figure 12. A surface is photographed in two different levels of stress. The reference image is subject to the observation of a tiny area (known as a sub-image), and after surface deformation, it is followed by the acquisition of a new image in which the corresponding sub-image from the previous state is sought. Cross-correlation techniques are used to determine the displacement between the two sub-images with accuracy that is a fraction of the camera's pixel size. The next step is to determine a motion vector for each sub-image. The algorithm creates the vectors, or N x N pixel matrices, that connect the locations of the sub-images in the second image to their locations in the reference image. The relative deformation of various specimen sections inside the optical system's field of vision is then computed into a matrix of sub-image deformation vectors.

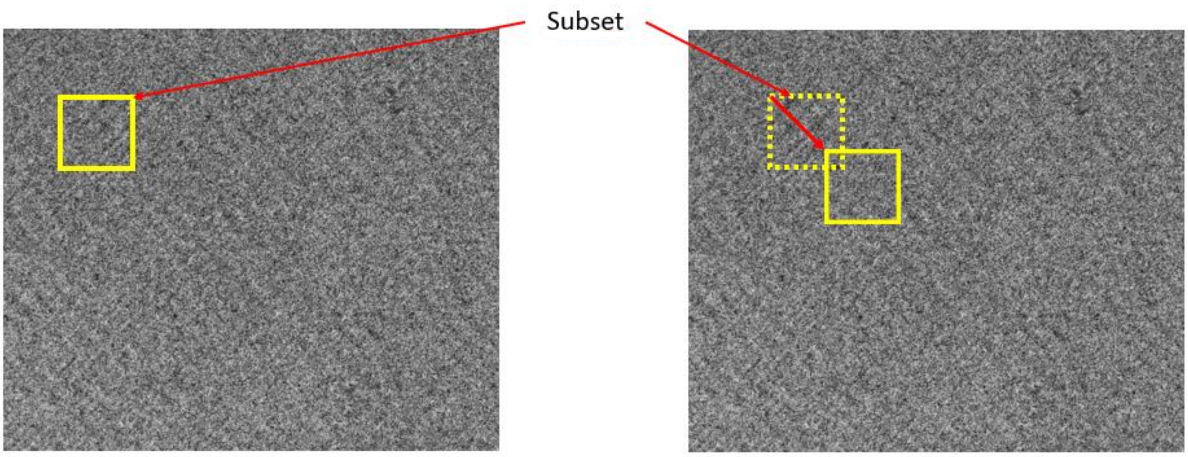

Figure 12 - Basic principle of Image Correlation

This measurement method has the advantage of having low sensitivity to external disturbances, resulting from its relatively low resolution. However, it’s sensitivity is limited by the resolution of the camera and by the measurement area.

2.6. Response surface Methodology

Characterizing the link between a response and a group of quantitative characteristics that are important to the researcher is a common objective in many different forms of experiments. To do this, a model that characterizes the reaction over the appropriate ranges of the relevant factors of interest is built. The fitted model is sometimes referred to as a response surface in industrial settings. The response surface can be investigated to identify key features like optimal operating conditions (i.e., factor values that yield the largest or smallest estimated response) or pertinent trade-offs when there are several responses (Mason et al, 2003).

In a variety of engineering problems, the response variable is expressed as an empirical function of one or more quantitative factors. In the context of this work, the residual stresses present in polymeric parts produced by additive manufacturing, could be expressed as a function of printing bed temperature, feed rate and layer height. A response function is used to simulate the relationship in order to achieve this:

$$Residual\ Stress = f(bed\ temperature, feed\ rate, layer\ height)$$

A generalized form of this type of response takes the form of:

$$y = f(x_1, x_2, \dots, x_k),$$

where $x_1, x_2, \dots, x_k$ are the quantitative levels of the factors of interest and y is the response. Understanding the form of the function, f, which can often be found by fitting models to data gathered from planned experiments, enables one to both summarize the experiment's findings and forecast the response for values of the quantitative components.

There are several important reasons to design experiments to study or fit responses, including:

- The response function is defined within an experimentally relevant region,

- Statistical inferences about the response's sensitivity to the factors of interest can be drawn,
- Factor levels can be identified for which the response variable is optimal (e.g., maximum, or minimum),
- Factor levels can be identified that simultaneously optimize multiple responses; if simultaneous optimization is not possible, tradeoffs are obvious (Mason et al, 2003).

2.6.1. Central Composite Design

A Central Composite Design (CCD) is a specific type of experimental design used in the context of Response Surface Methodology. It is commonly used in statistics and engineering to explore the relationships between multiple variables and optimize a response variable. It is particularly useful when the relationship between the variables is not well understood, and the goal is to determine the optimal conditions to achieve a desired outcome.

During the CCD experiment, multiple runs are conducted to investigate the relationship between the input variables and the response variable of interest. The response variable's values obtained from these experimental runs can vary due to various factors, including experimental error, natural variability, and other uncontrollable influences.

Once the experimental runs are completed, the collected data is analysed statistically to calculate various parameters and estimate the response surface model. One of the key metrics used to assess the variability in the response data is the standard deviation (S). It measures how much individual data points deviate from the mean or central value. A higher "S" indicates greater variability, while a lower "S" suggests more consistency in the response variable's values.

A Central composite design construction goes according to the following steps:

1. Depending on the necessity for efficiency and the capacity to disregard interaction effects, construct a complete or fractional 2^k factorial arrangement,
2. The coordinate axes should be extended by $2k$ axial, or star, points,
3. Add m repeat observations at the design center,
4. Depending on what is appropriate, allocate factor-level combinations randomly to the experimental units or the run sequence.

A central composite design based on a full $2k$ factorial has $n = 2^k + 2k + m$ test runs overall. Since this count is typically lower than 3^k, fewer observations are needed than for a 3^k factorial. Choosing $a = F^{\frac{1}{4}}$, where F is the number of factorial points (e.g., $F = 2^k$ when a complete factorial is employed), can be used to make the central composite design rotatable. In this design, a is a constant, which can be chosen to make the design notable or to satisfy some other desirable property. Its value determines the distance of the axial points from the center and influences the precision and characteristics of the estimated response surface. Figure 12 provides an instance of an entire 2^k factorial-based three-factor central composite design (Mason et al, 2003).

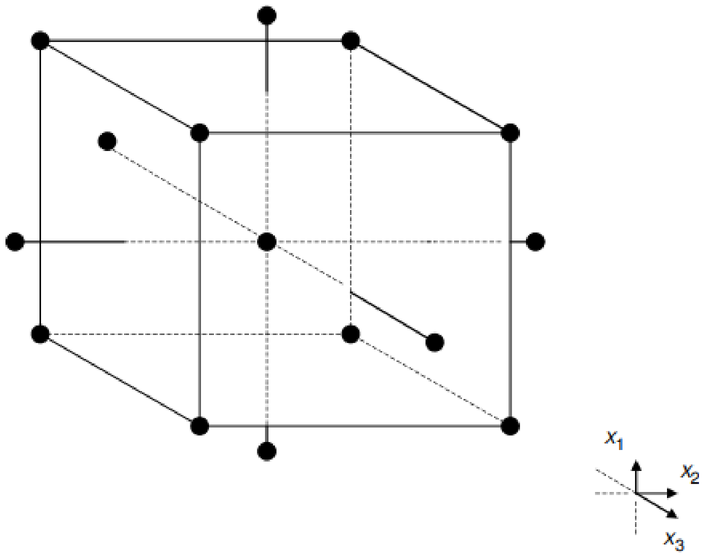

Figure 13 - Central Composite Design with three factors (Mason et al, 2003).

3. Methodology

The residual stress determination process included four steps as can be seen in the diagram in Figure 14.

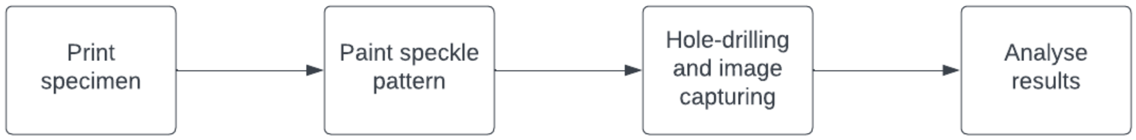

Figure 14 - Methodology applied to determine residual stresses in the specimens.

A design of experiments (DoE) was created to determine the influence of a select number of printing parameters on the resulting residual stresses present in the specimens in analysis. This method includes a number of applied statistics tools that are used to systematically categorize and quantify cause-and-effect relationships between inputs and outputs in the studied process or phenomenon, which leads to the discovery of the conditions and variables that lead to the process's optimum performance (Jankovic et al, 2021). In this case, the response surface design with extrusion temperature, feed rate and printed layer height as varying factors present in table 2 was created.

Table 2 - Design of Experiments created to determine the influence of printing parameters in residual stresses.

StdOrder	RunOrder	PtType	Blocks	Extrusion Temperature (ºC)	Feed rate (mm/s)	Layer Height (mm)
3	1	1	1	238	52	0,15
19	2	0	1	250	40	0,23
17	3	0	1	250	40	0,23
9	4	-1	1	230	40	0,23
13	5	-1	1	250	40	0,10
8	6	1	1	262	52	0,30
12	7	-1	1	250	60	0,23
14	8	-1	1	250	40	0,35
20	9	0	1	250	40	0,23
7	10	1	1	238	52	0,30
6	11	1	1	262	28	0,30
2	12	1	1	262	28	0,15
16	13	0	1	250	40	0,225
4	14	1	1	262	52	0,15
1	15	1	1	238	28	0,15
18	16	0	1	250	40	0,23
15	17	0	1	250	40	0,23
10	18	-1	1	270	40	0,23
11	19	-1	1	250	20	0,23
5	20	1	1	238	28	0,30

The resulting three-factor central composite design has an alpha value of $\alpha = 1.682$, the boundary conditions present in table 3 and the order of the experiments was randomized to minimize the influence of biases associated with the printing process.

Table 3 - Varying factors in the Design of Experiments.

Varying factor	Minimum value	Maximum value
Extrusion Temperature (ºC)	270	230
Feed rate (mm/s)	20	60
Layer Height (mm)	0.10	0.30

The remaining printing parameters were constant for all of the specimens produced and the most notable ones are present in table 4 below.

Table 4 - Constant printing parameters.

Parameter	Value Chosen
Infill pattern	Rectilinear
First layer height	0.2mm
Perimeters	2
Bed Temperature	80ºC
First layer extrusion temperature	230ºC
Infill percentage	100%

The printed parts were 80×40×7mm in dimension as can be seen in figure 15 and a 1.5mm hole was drilled to a depth of 1mm in each specimen.

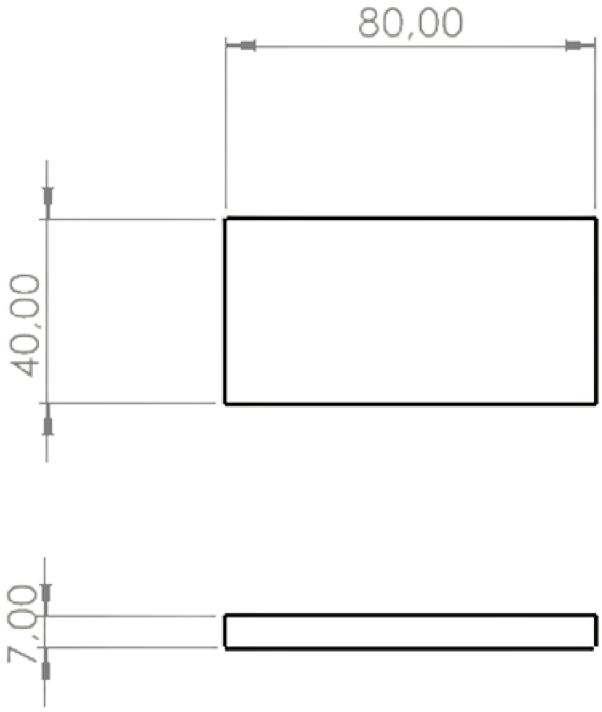

Figure 15 - Dimensions of the printed specimen.

The printer used was a Prusa i3 MK3S pictured in Figure 16.

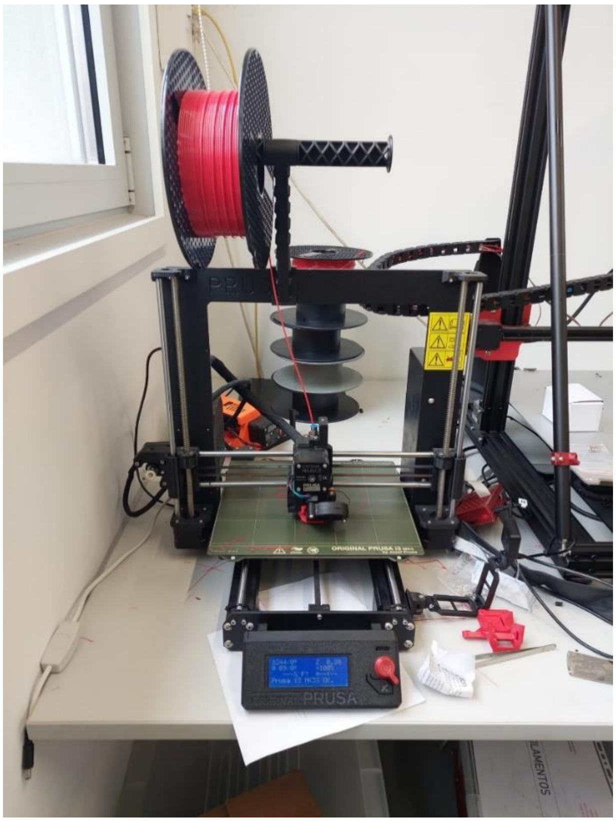

Figure 16 - Prusa i3 MK3S 3D printer.

After printing the specimens, a speckle pattern was painted on them using an airbrush in order to track the surface displacements while proceeding with the hole drilling process as seen on Figure 17.

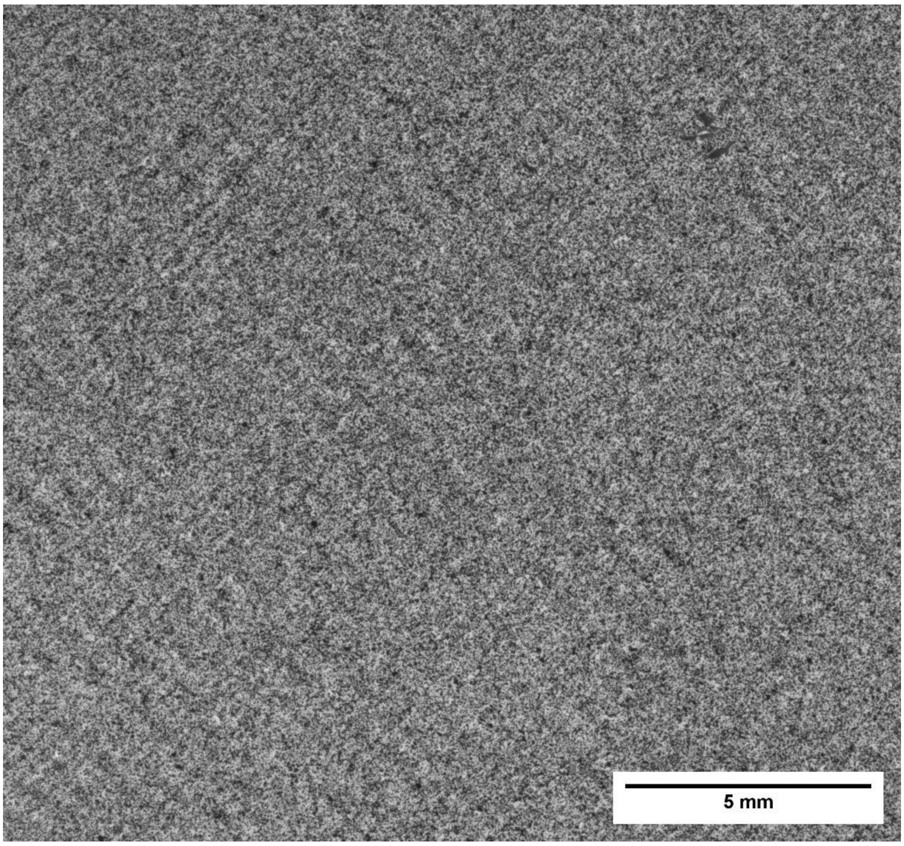

Figure 17 - Example of a speckle pattern painted on the specimens.

The holes were drilled using the MTS3000-Restan automatic system for hole-drilling measurements by SINT Technology (figure 18).

Figure 18 - Automatic system for the measurement of residual stresses, MTS3000-Restan (SINT Technology, 2021).

The drilling device in question complies with ASTM 837-08's standard test method for determining residual stresses method, by being able to drill a hole aligned concentric with the strain gage circle to within $\pm 0.004D$, with D being the drilled hole's diameter. Additionally, it is also able to control the depth of the hole to $\pm 0.004D$.

The drilling was done by plunging, where the cutter is advanced axially in 14 drilling increments to guarantee the process was done under constant temperature conditions. After each drilling step, the cutter was stopped to allow time for stabilization of any potential temperature fluctuations caused by the drilling process itself, or the air turbine exhaust, whilst also allowing for the displacement images to be taken. Images of the surface of each specimen were captured initially, before the drilling process, and also after each drilling increment. A drilled hole example is present in figure 19.

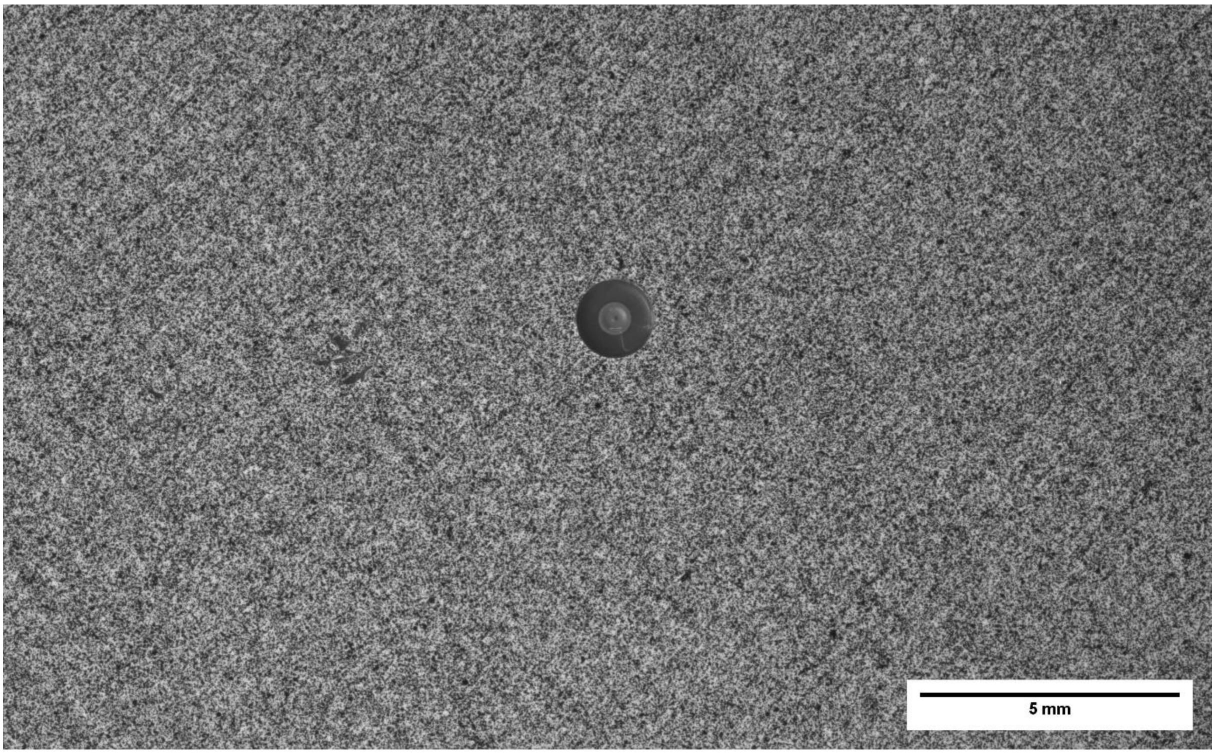

Figure 19 - Drilled hole on printed specimen.

The experimental setup of the drilling and image acquisition process can be seen in Figure 20, which included the aforementioned MTS3000-Restan drilling machine; a Basler ace acA5472-17um camera, with a 15.8 mm diagonal sensor size, and a 20 Megapixel resolution (5472 px x 3648 px); a light source; and a computer to control the drilling process.

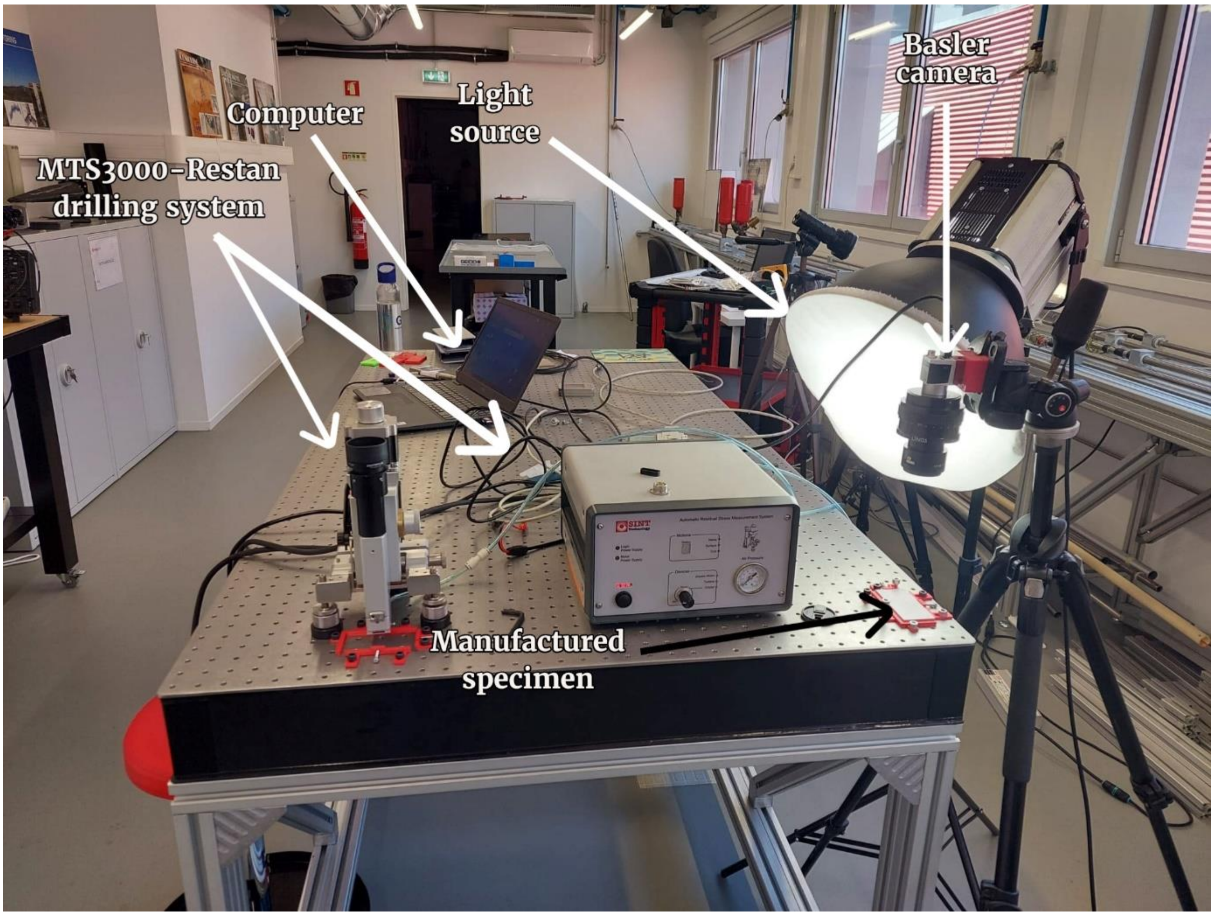

Figure 20 - Experimental drilling and image acquisition setup.

The displacements on the surface of the specimens were measured using virtual extensometers in Correlated Solutions' VIC-2D software, which utilizes correlation algorithms to provide non-contact, full-field, two-dimensional displacement and strain data for mechanical testing on planar specimens (Correlated Solutions, 2023).

The virtual extensometers were placed in the same locations as a conventional strain gage rosette as seen in Figure 21 and strain measurements on the surface were taken for each drill increment.

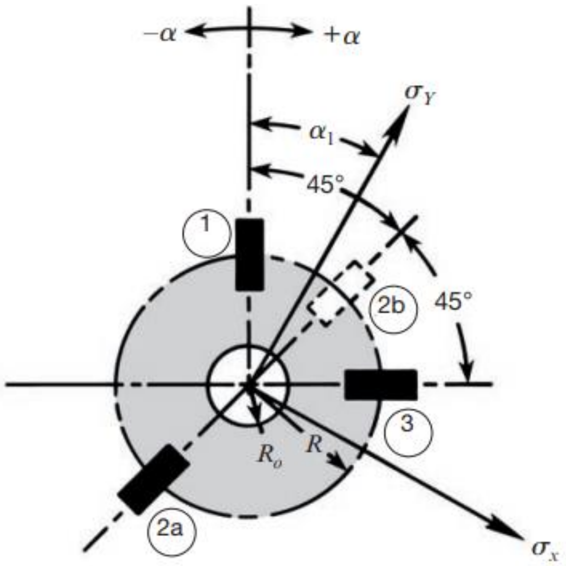

Figure 21 - Strain gage rosette arrangement for determining residual stresses (Vishay Precision Group, 1993).

The conversion of the displacements into stresses was done using the integral method on SINT Technology's EVAL 7 software.

3.1. Integral method

In many cases, the gradients of residual stresses in depth assume special importance, as the amplitude of residual stresses varies from a maximum value at the surface to zero. The method described in previous chapters cannot be applied to this case, as it only allows for the measurement of the average values of residual stress along the depth of the hole. In order to characterize the distribution of non-uniform residual stresses in depth, the hole must be drilled incrementally. The methods of average stresses and incremental deformation, used as approximations in the strain gauge method, cannot be applied in Digital Image Correlation. For this case, it is necessary to use the integral method described in Chapter 2, as the relaxed residual stresses at each drilling stage produce strong nonlinear contributions to the existing displacement field (Ribeiro, 2006).

The distribution of non-uniform residual stresses in depth can be determined by the integral method introduced earlier. When a hole is drilled incrementally, the surface displacements can be continuously measured around the hole using DIC. If the increase in depth of the blind hole is known, the residual stress of each drilled increment is considered as a uniform distribution with an amplitude corresponding to the average value (Ribeiro, 2006).

Starting from the strains $\varepsilon_{1,j}, \varepsilon_{2,j}, \varepsilon_{3,j}$ acquired for a drilling step j, the following combination of strains have to be calculated:

$$p_j = \frac{(\varepsilon_3 + \varepsilon_1)_j}{2} \tag{3.1}$$

$$q_j = \frac{(\varepsilon_3 - \varepsilon_1)_j}{2} \tag{3.2}$$

$$t_j = \frac{(\varepsilon_3 + \varepsilon_1 - 2\varepsilon_2)_j}{2} \tag{3.3}$$

From this strain combination, it is possible to show that the evaluation of residual stresses can be obtained by the following integral equations:

$$p(h_j) = \frac{1+\nu}{E}\int_0^{h_j} \hat{A}(H, h_j) * P(H)dH \tag{3.4}$$

$$q(h_j) = \frac{1}{E}\int_0^{h_j} \hat{B}(H, h_j) * Q(H)dH \tag{3.5}$$

$$t(h_j) = \frac{1}{E}\int_0^{h_j} \hat{B}(H, h_j) * T(H)dH \tag{3.6}$$

Where Â and $\hat{B}$ are influence functions for equibiaxial and shear stress to take into account the effect of relieved stresses at depth H of an h_j depth hole (Sint Technology, 2014).

4. Results

4.1. Comparison between Traditional and DIC approaches

Specimens 1 and 2 in the run order were printed twice each and the principal residual stresses in these were measured once using strain gages and once using the DIC approach.

To test the accuracy of the suggested method, two specimens were tested using traditional type A strain gage rosettes (CEA-062UL-120 by Vishay micro-measurements), as seen in Figure 22.

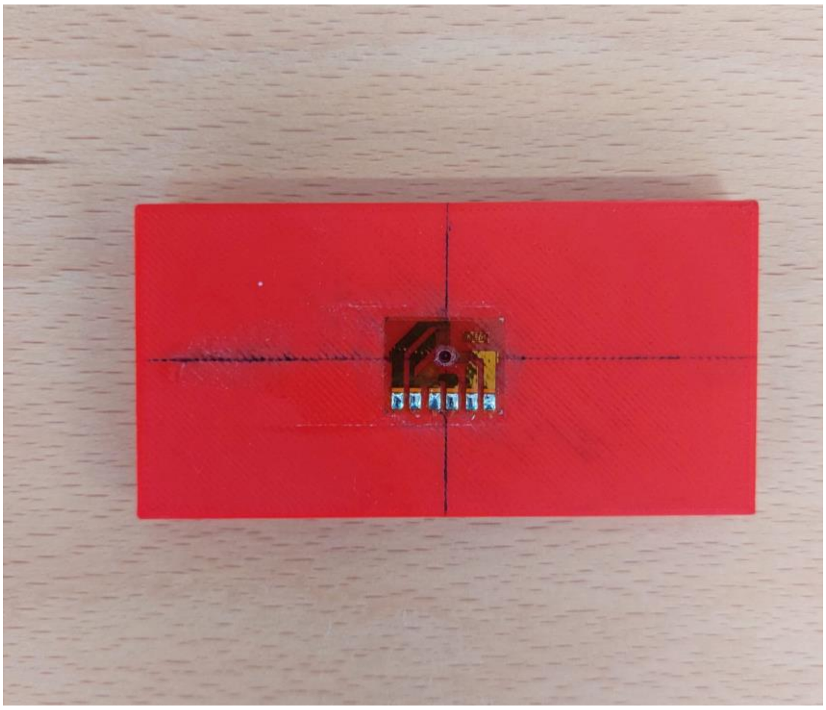

Figure 22 - Strain gage rosette mounted on printed specimen.

In comparison, Figure 23 presents a drilled specimen with a painted speckle pattern, used for the DIC strain measurement approach.

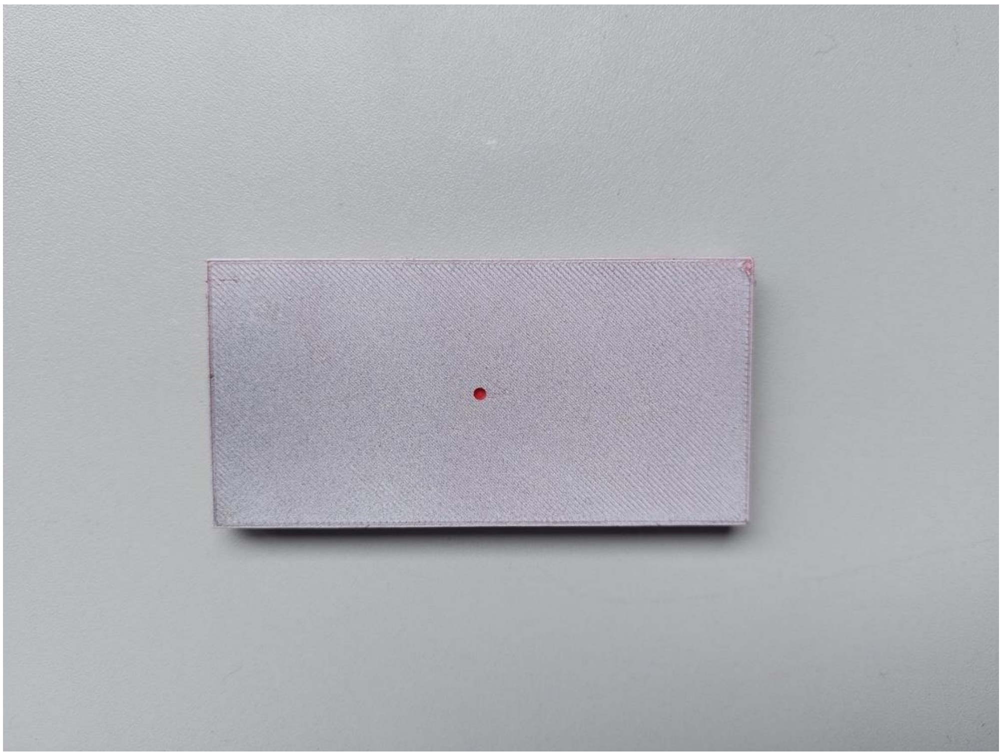

Figure 23 - Drilled specimen used for the DIC strain measurement approach.

The results from this comparison are presented below.

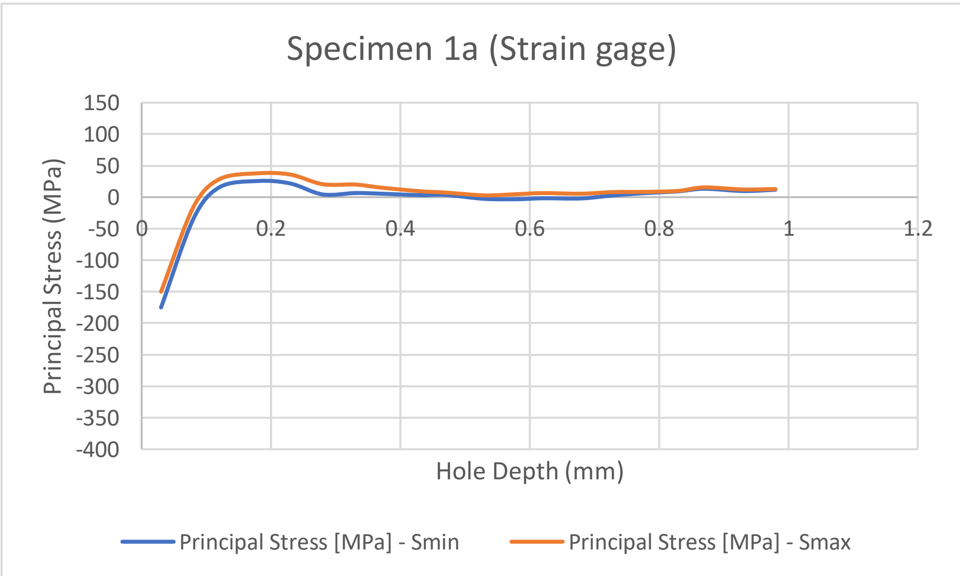

Figure 24 - Principal stresses in Specimen 1a, obtained using strain gage measurement.

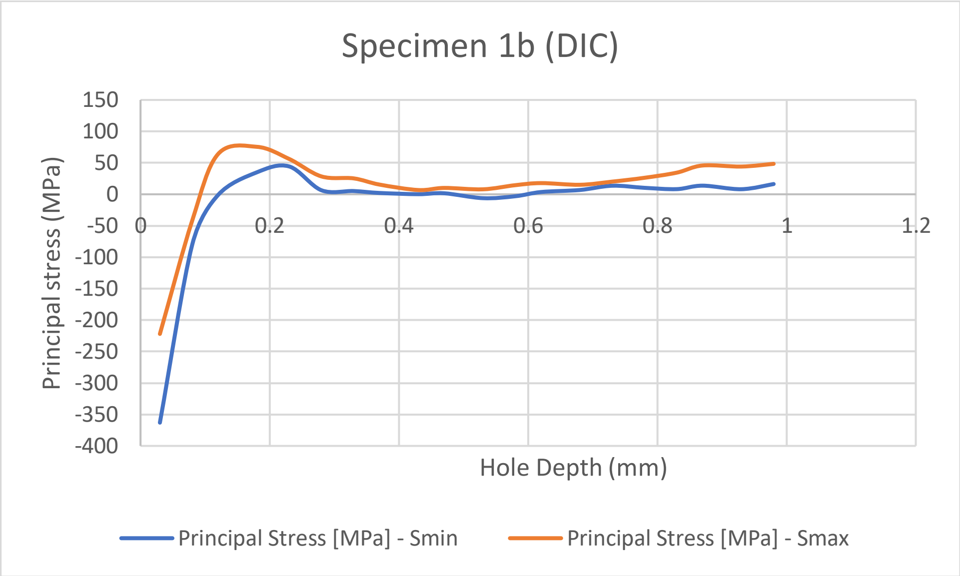

Figure 25 - Principal stresses in Specimen 1b obtained using DIC measurement.

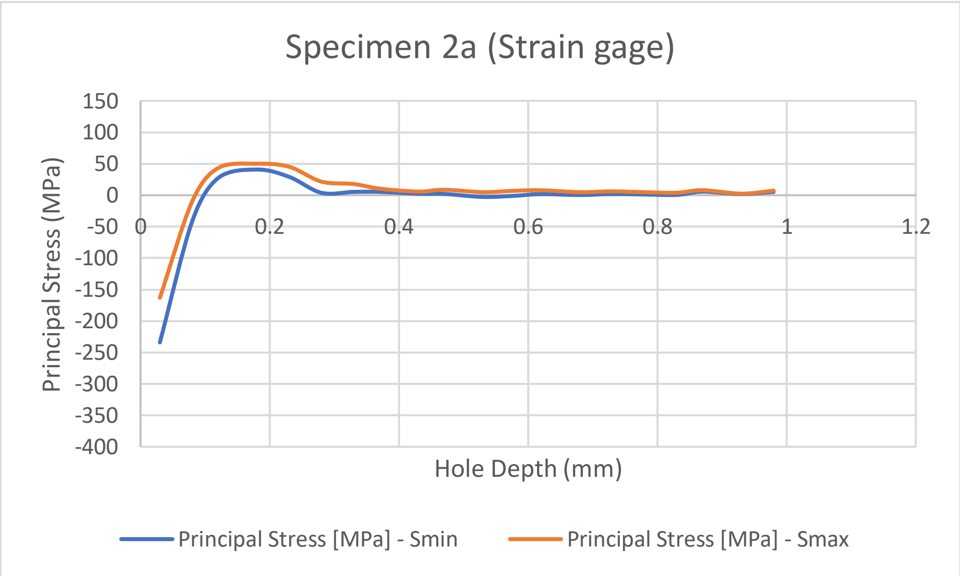

Figure 26 - Principal stresses in Specimen 2a obtained using strain gage measurement.

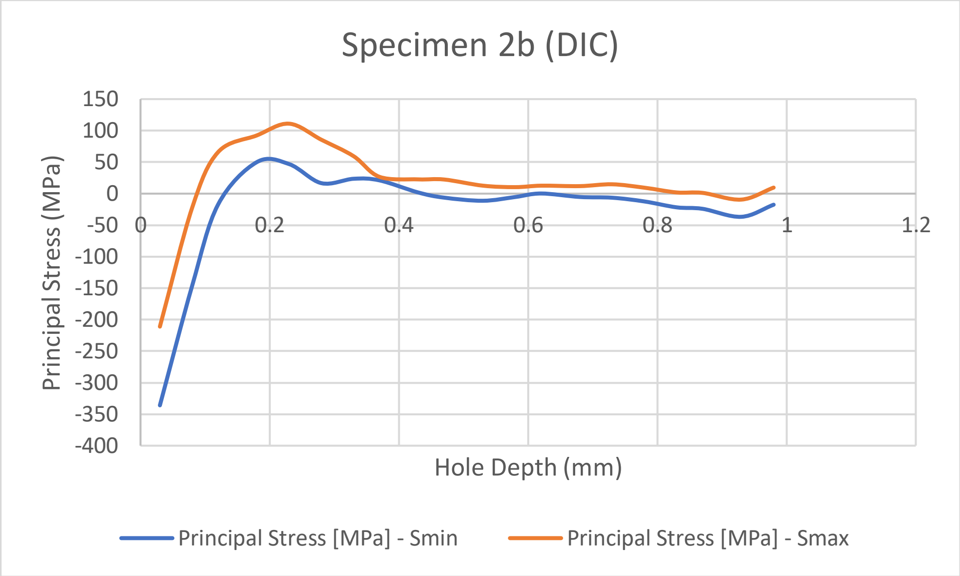

Figure 27 - Principal stresses in Specimen 2b obtained using DIC measurement.

As can be seen in figures 24-27, the principal stresses over hole depth plots follow a similar shape, as with Type A rosettes, where sensitivity for stresses over 0.2D depth decreases to almost zero, with the measured strains mostly being dependent on the near-surface stresses. Thus, around 0.2mm to 0.3mm deep from the observed surface, hole-drilling data show a weighted average of the residual stresses in the near-surface layer (ASTM, 2013).

However, despite having the same general shape, there is a discrepancy between the maximum values registered for the stresses using both methods. It can be observed that the stresses obtained through the DIC approach are slightly higher than those measured using the strain gages.

Using the Von Mises principal plane stress equation below to calculate the equivalent stress in all four situations, the results in table 5 were obtained.

$$\sigma_V = \sqrt{\sigma_1^2 + \sigma_2^2 - \sigma_1\sigma_2} \tag{3.7}$$

Table 5 - Equivalent principal plane stress of each specimen.

Specimen	**Equivalent Stress (MPa)**
Specimen 1 (Strain gage)	31.32
Specimen 1 (DIC)	65.44
Specimen 2 (Strain gage)	46.09
Specimen 2 (DIC)	96.51

Considering the yield strength of the material is between 47.9 and 52.9 MPa, the equivalent stresses obtained through the DIC approach seem particularly large. However, these are due to the fact that the extensometers present in physical strain gage rosettes measure the strains across the area where they are placed, with the resulting output being an average of the strains across the entire section. On the other hand, when using virtual extensometers, the resulting strains depend only on the displacement of the two points on the extremities of these virtual instruments as is illustrated in Figure 28 below.

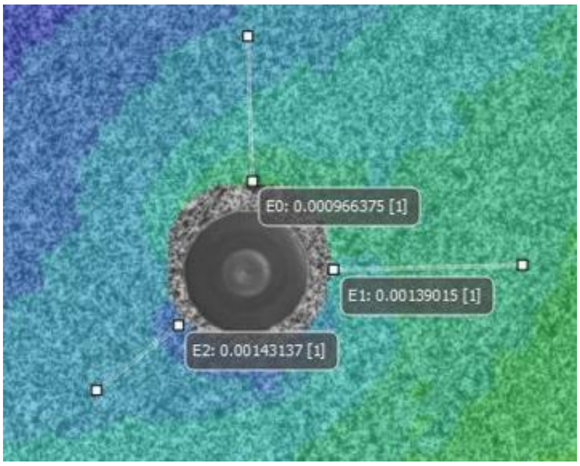

Figure 28 - Strain gage rosette formed with virtual extensometers.

This leads to the difference between results originating from the physical strain gages as opposed to their digital counterparts.

In an attempt to confirm this, the residual stresses in specimens 1 and 2 were again measured using DIC, except this time with one difference. The virtual extensometers were replaced with strain measurement averages across small areas in the same positions as displayed in Figure 21, with the extensometer number 1 represented in the figure measuring strains in the y axis, extensometer number 3 measuring strains in the x axis and strains in the area of extensometer 2a being calculated through the following expression:

$$\varepsilon = \frac{\varepsilon_x + \varepsilon_y}{2} + \sqrt{\left(\frac{\varepsilon_x - \varepsilon_y}{2}\right)^2 + \left(\frac{\gamma_{xy}}{2}\right)^2} \tag{3.8}$$

The results for these measurements are presented in Figures 29 and 30.

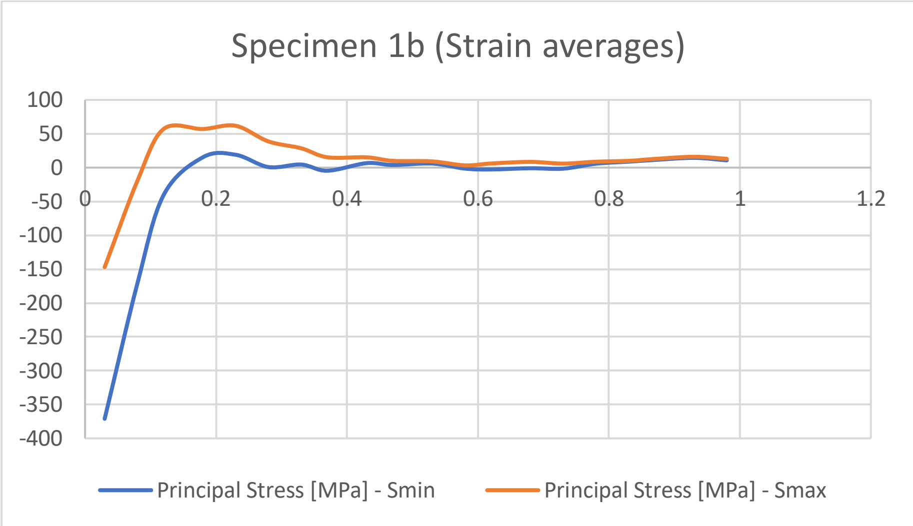

Figure 29 - Principal stresses in Specimen 1b obtained using DIC measurement with strain averages.

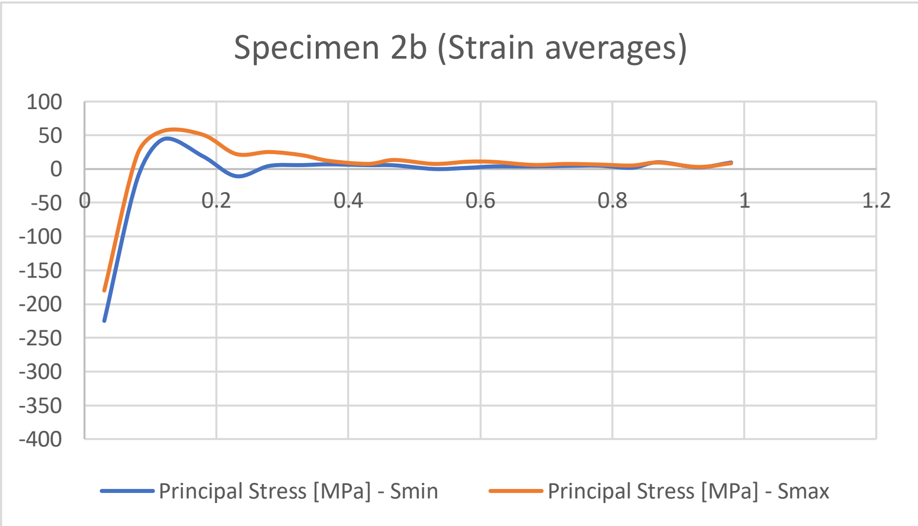

Figure 30 - Principal stresses in Specimen 2b obtained using DIC measurement with strain averages.

Using this approach, the resulting equivalent stresses are 54.83 MPa for specimen 1b and 51.63 MPa for specimen 2b. A 16% reduction in equivalent stress for the first case and 47% reduction for the second case, bringing the results closer to those obtained using the physical strain gages.

The strains calculated through the averages within predefined areas produced results more similar to those from the physical strain gages. However, the results presented in the following sections derived from the use of standard virtual extensometers, as both approaches are considered to be valid, with the difference residing in the larger amount of data being collected in the first approach, leading to generally slightly lower residual stress values. Furthermore, the initial shape of the curves in Figure 29 lead to believe that the results were influenced by outliers or DIC processing errors, which could explain why the equivalent stress value reduction wasn´t as significant as with specimen 2. This fact further incentivized the use of regular virtual extensometers for the remaining analysis, as they appear to be more immune to these types of errors.

4.2. DoE Results

The stepwise backward elimination method was used to remove and add terms to the model for the purpose of identifying a useful subset of the terms. This method starts with all potential terms in the model and removes the least significant term for each step. The Minitab software, used to perform this analysis, stops the elimination process when all variables in the model have p-values that are less than or equal to the specified Alpha to remove value. In this case, $\alpha = 0.1$.

4.2.1. Statistical significance between the response and the terms

A comparison of the p-value for each term to the significance level to evaluate the null hypothesis to see if there is a statistically significant relationship between the response and each term in the model was done, as seen in tables 6 and 7. The null hypothesis is that there is no association between the term and the response since the term's coefficient is equal to zero. A significance level of 0.1 was considered.

Table 6 - Analysis of variance of the minimum principal stress.

Analysis of Variance

Source	DF	Adj SS	Adj MS	F-Value	P-Value
Model	4	6476,8	1619,2	4,92	0,010
Linear	2	2733,3	1366,7	4,15	0,037
Extrusion Temperature	1	1736,5	1736,5	5,27	0,036
Feed rate	1	996,8	996,8	3,03	0,102
Square	1	2362,7	2362,7	7,18	0,017
Feed rate*Feed rate	1	2362,7	2362,7	7,18	0,017
2-Way Interaction	1	1380,8	1380,8	4,19	0,059
Extrusion Temperature*Feed rate	1	1380,8	1380,8	4,19	0,059
Error	15	4938,8	329,3		
Lack-of-Fit	10	3632,7	363,3	1,39	0,376
Pure Error	5	1306,1	261,2		
Total	19	11415,6			

Table 7 - Analysis of variance of the maximum principal stress.

Analysis of Variance

Source	DF	Adj SS	Adj MS	F-Value	P-Value
Model	3	21561	7187	1,55	0,241
Linear	2	6170	3085	0,66	0,528
Extrusion Temperature	1	4936	4936	1,06	0,318
Feed rate	1	1234	1234	0,27	0,613
2-Way Interaction	1	15391	15391	3,31	0,088
Extrusion Temperature*Feed rate	1	15391	15391	3,31	0,088
Error	16	74353	4647		
Lack-of-Fit	11	27072	2461	0,26	0,971
Pure Error	5	47281	9456		
Total	19	95914			

It can be concluded that there is a statistically significant correlation between the response variable and the term if the p-value is less than or equal to the significance level. If the p-value is greater than the significance level, you cannot conclude that there is a statistically significant association between the response variable and the term.

If a coefficient for a factor is significant, as is the case for the extrusion temperature in σ_2 response, it can be concluded that not all level means are equal. If a coefficient for a squared term is significant, as happens with the squared feed rate term in the σ_2 response, then the relationship between the factor and the response follows a curved line. The link between a factor and the response is dependent on the other factors in the term if a coefficient for an interaction term is significant. This can be observed in the extrusion temperature and feed rate interactions in σ_2 and σ_1 responses (Minitab, 2023).

4.2.2. Variability in the response

Pareto charts of the standardized effects are used to compare the relative magnitude and the statistical significance of main, square, and interaction effects. The chart displays the absolute value of the standardized effects. Below, in figures 31 and 32 are presented the pareto charts of the standardized effects on the minimum and maximum principal stresses.

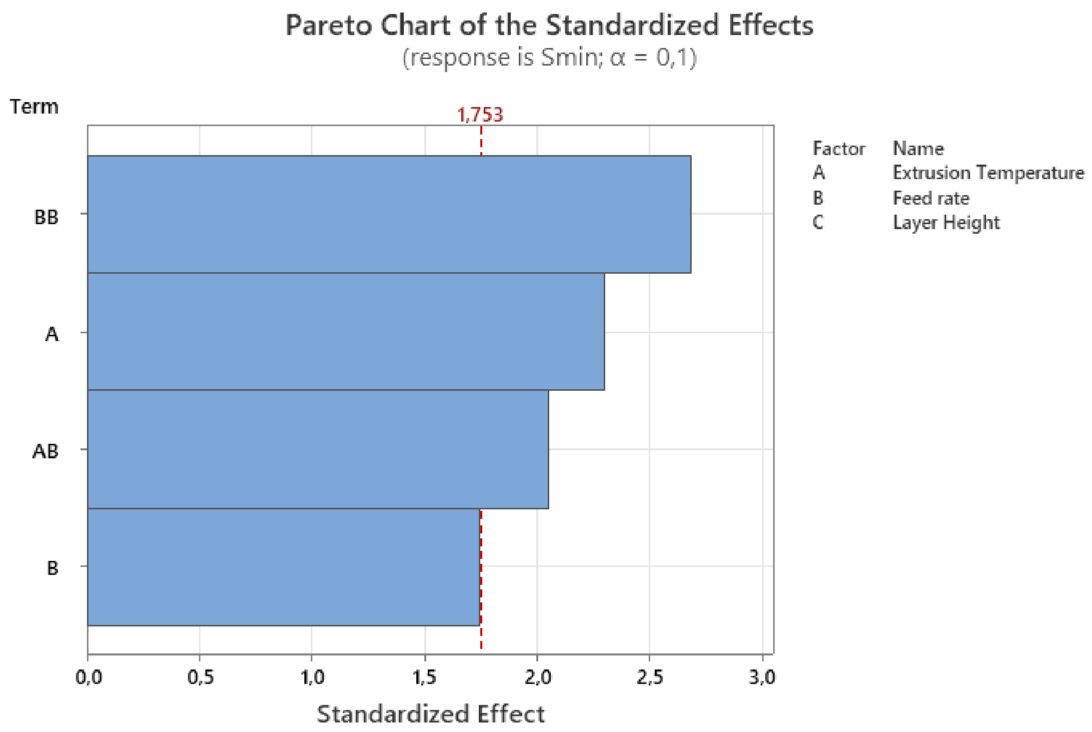

Figure 31 - Pareto chart of the standardized effects on the minimum principal stress.

In these results, the squared term for feed rate (BB), the interaction between extrusion temperature and feed rate (AB) and the Extrusion temperature term (A) are significant at the α= 0.1 significance level. No significant terms including the Layer Height factor (C) were identified during the DOE analysis. This factor was eliminated through stepwise backward elimination.

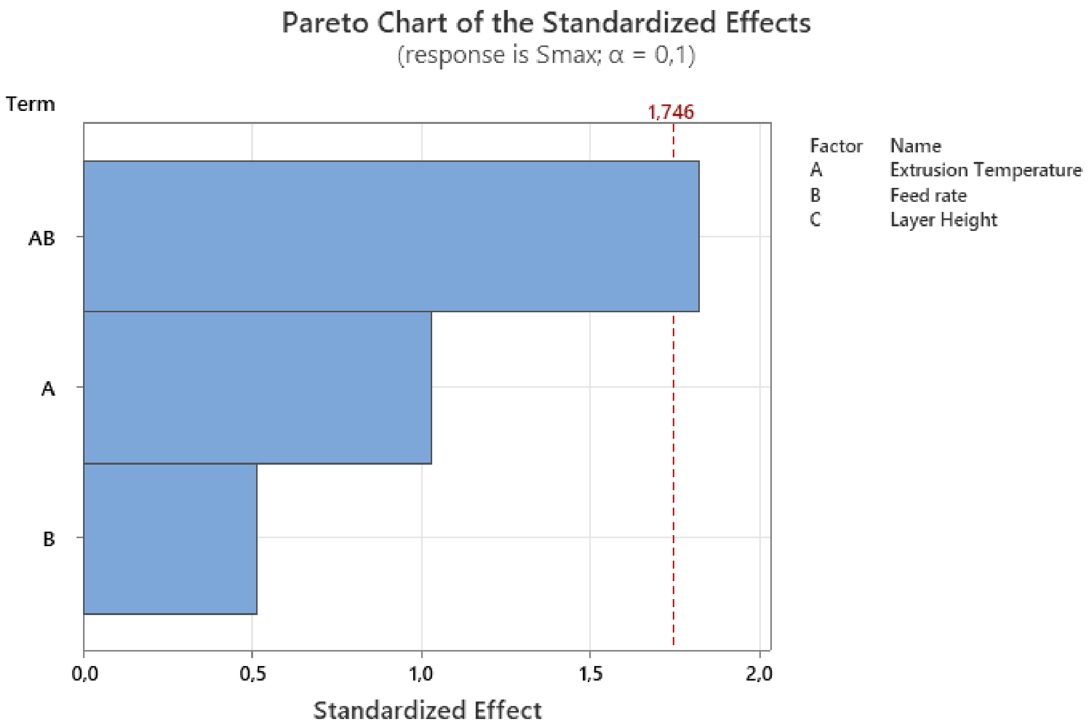

Figure 32 - Pareto chart of the standardized effects on the maximum principal stress.

When it comes to the results for the maximum principal stress, again the interaction between extrusion temperature and feed rate (AB) is significant, making it the only significant term for this response analysis.

4.2.3. Residual plots

The residual plots aid in assessing the model's suitability and compliance with the analysis's underlying assumptions. The model might not adequately match the data if the assumptions are not met.

The premise that the residuals are independent from one another is validated using the residuals versus order plot. When exhibited in time order, independent residuals do not exhibit any trends or patterns. Patterns in the data may suggest that residuals close to one another are likely correlated and therefore not independent. The residuals on the plot should ideally be distributed randomly around the centre line. The Versus order plots for the minimum and maximum principal stresses are presented in Figures 33 and 34 (Minitab, 2023).

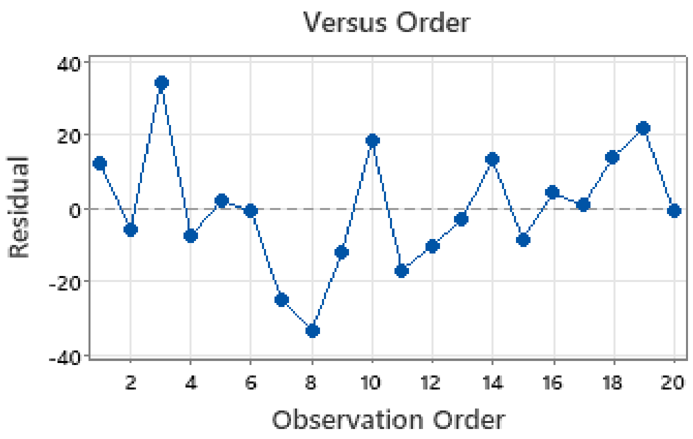

Figure 33 – Residuals versus order plot for minimum principal stress.

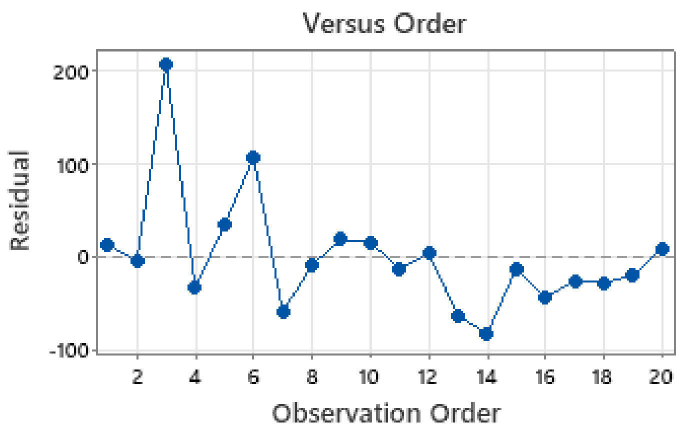

Figure 34 - Residuals versus order plot for maximum principal stress.

The residuals versus fits graph plots the residuals on the y-axis and the fitted values on the x-axis. To confirm the notion that the residuals are equally distributed and have a constant variance, the residuals versus fits plot is used. The points should ideally be distributed randomly on both sides of 0, with no discernible patterns, as seen in figures 35 and 36.

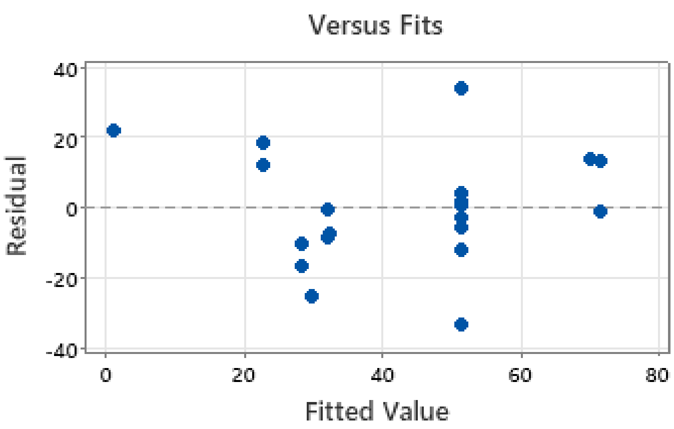

Figure 35 - Residuals versus fits plot for minimum residual stress.

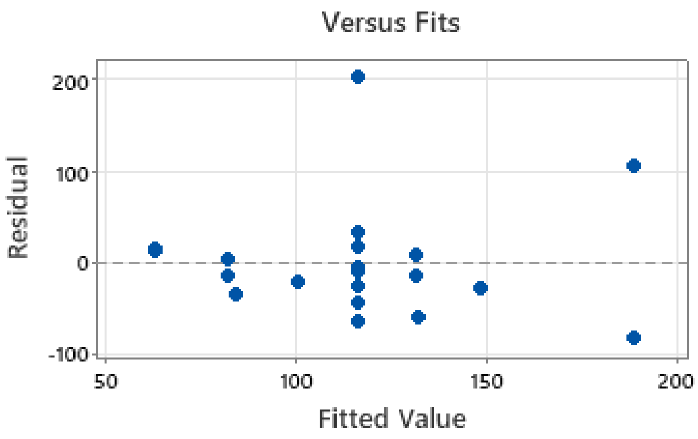

Figure 36 - Residuals versus fits plot for maximum residual stress.

The assumption that the residuals are normally distributed is confirmed using the normal probability plot of the residuals. The residuals' normal probability plot should roughly approximate a straight line like the ones presented in figures 37 and 38 below.

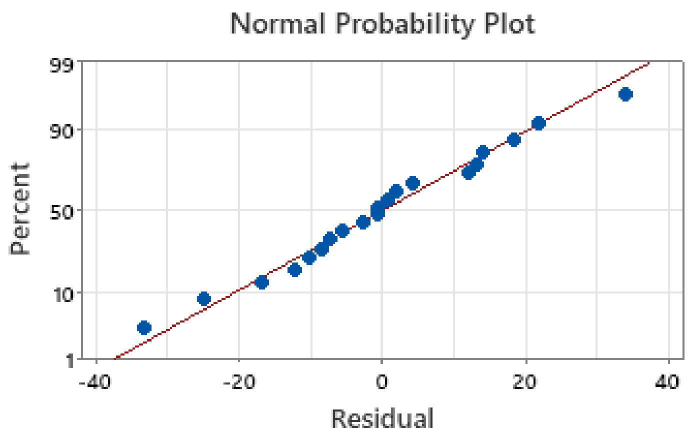

Figure 37 - Normality probability plot of the residuals for minimum principal stress.

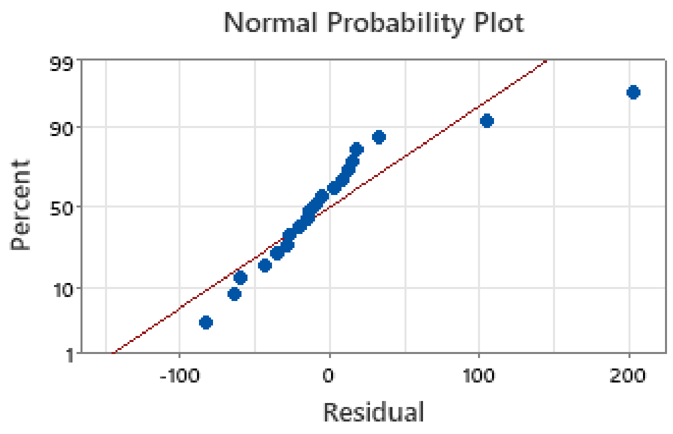

Figure 38 - Normality probability plot of the residuals for maximum principal stress.

Through the analysis of this information, it is possible to conclude that the residuals are independent from one another, apart from being equally distributed, having a constant variance and are normally distributed.

4.2.4. Models' summary

Model summaries for both σ_2 and σ_1 responses are presented in tables 8 and 9 below, along with their respective regression equations. These help to determine how well the model fits the data.

Table 8 - Model summary for the minimum principal stress response.

Model Summary

S	R-sq	R-sq(adj)	R-sq(pred)
18,1454	56,74%	45,20%	0,00%

$$\sigma_2 = 571 - 2{,}77\ Extrusion\ Temperature - 15{,}3\ Feed\ rate - 0{,}0897\ Feed\ rate * Feed\ rate + 0{,}0929\ Extrusion\ Temperature * Feed\ rate \quad (3.9)$$

Table 9 - Model summary for the maximum principal stress response.

Model Summary

S	R-sq	R-sq(adj)	R-sq(pred)
68,1695	22,48%	7,94%	0,00%

$$\sigma_1 = 2786 - 10{,}81\ Extrusion\ Temperature - 76{,}7\ Feed\ rate + 0{,}310\ Extrusion\ Temperature * Feed\ rate \quad (3.10)$$

S reflects the variation in how much the data values deviate from the genuine response surface and is expressed in the units of the response variable. The better the model describes the response, the lower the value of S. Opposite to S, the higher the R^2 value, the better the model fits your data, with it always falling between 0% and 100%. Adjusted R^2 is used when a comparison is needed between models that have different numbers of predictors and predicted R^2 is used to determine how well the model predicts the response for new observations. If the predicted R^2 is significantly lower than R^2, the model may be over-fit. When terms are included for effects that are not significant in the population, the model becomes over-fit. Predictions regarding the population may not be useful since the model becomes customized to the sample data (Minitab, 2023).

Contour plots of the extrusion temperature and feed rate are presented in figures 39 and 40 below since this interaction presents itself as the only significant one.

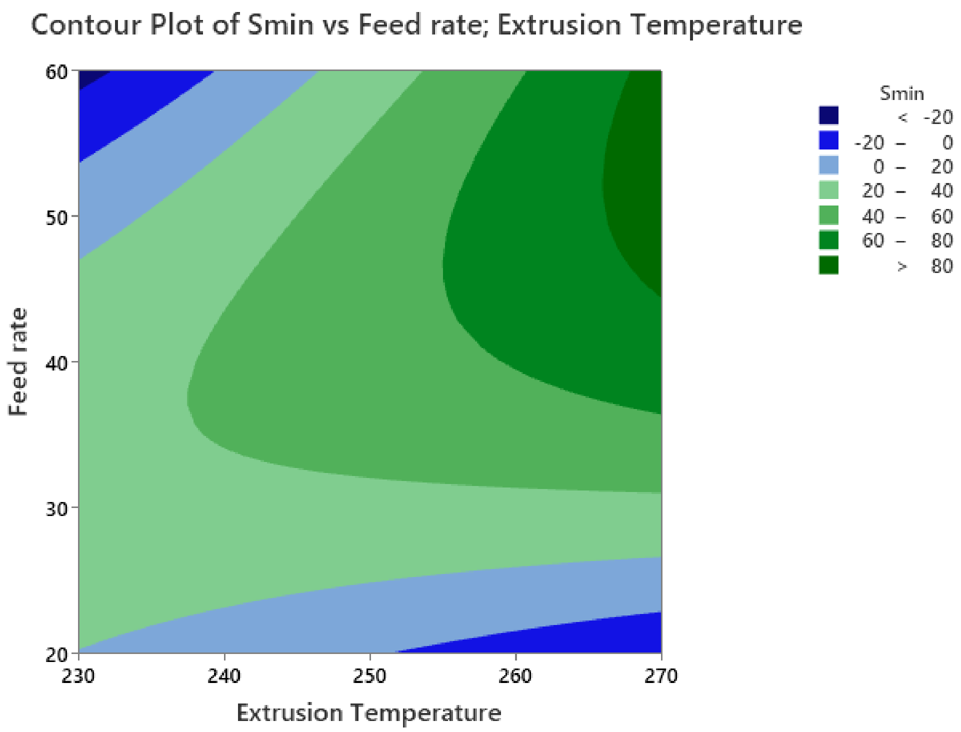

Figure 39 - Contour plot of minimum residual stress vs. feed rate and extrusion temperature.

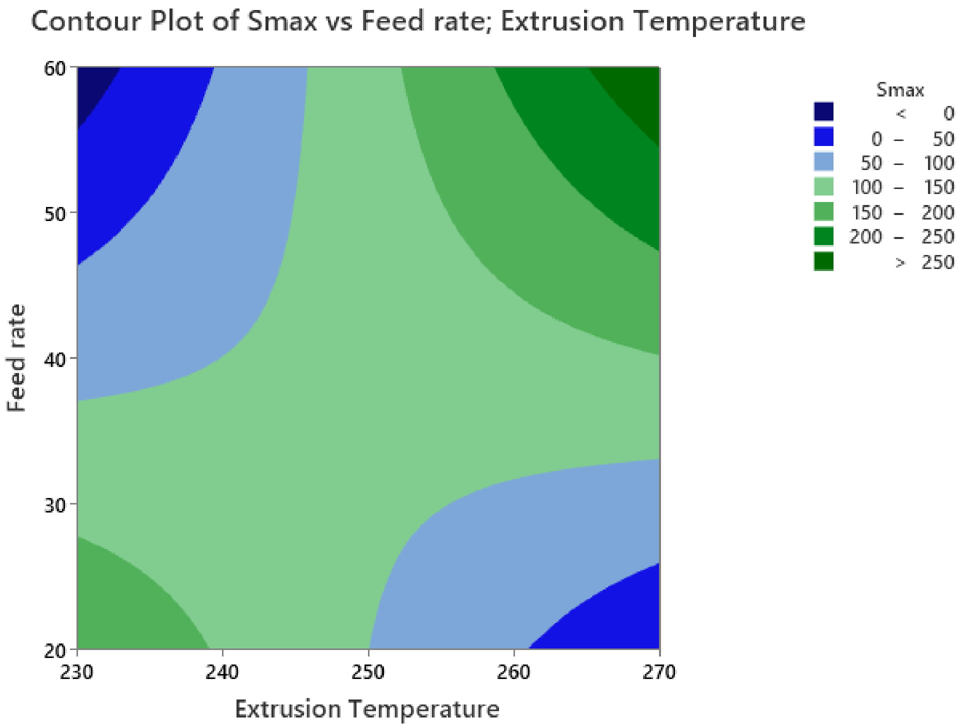

Figure 40 - Contour plot of maximum residual stress vs. feed rate and extrusion temperature

These plots represent two-dimensional views in which points that have the same response value are connected to produce contour lines. They are used when the relationship between a fitted response and two continuous variables is to be visualized for a specific model.

The parameter values to minimize the formation of residual stresses on the printed specimens are presented in table 10.

Table 10 - Paremeter values which minimize the formation of residual stresses.

Parameter	Value
Extrusion Temperature	230 °C
Feed rate	60 mm/s

As can be observed from the information above, the model for σ_2 fits the data better than the σ_1 model, presenting both a lower value of S as well as a higher value of R^2. This discrepancy in the results may be associated with the fact that in polymers, the behaviour under stress can be complex due to their molecular structure and mechanical properties. The complexity of this behaviour can be further amplified when considering additive manufacturing of polymers. The difference in the behaviour of maximum principal stress and minimum principal stress in polymers is primarily attributed to their anisotropic nature and the presence of molecular chains.

Polymers are made up of long chains of repeating molecular units, which can have different orientations and alignments. These chains can slide past each other to some extent when the material is subjected to stress. This sliding motion is relatively easier along certain directions or planes and more difficult along others. Consequently, the material exhibits anisotropic behaviour, meaning its properties are directionally dependent. the stress distribution within the material is not uniform. Instead, it is influenced by the molecular alignment and the direction of the applied stress.

The maximum principal stress corresponds to the direction of the applied stress where the material experiences the highest magnitude of stress. On the other hand, the minimum principal stress corresponds to the direction perpendicular to the maximum principal stress, where the material experiences the lowest magnitude of stress. Due to the anisotropic nature of polymers, the alignment and orientation of molecular chains can vary throughout the material. This variability can cause the maximum principal stress to be more erratic compared to the minimum principal stress. The chains may align differently in different regions of the material, leading to variations in the magnitude and direction of the maximum principal stress.

Moreover, polymers often exhibit nonlinear stress-strain behaviour, where the relationship between stress and strain is not linear. This nonlinearity may further contribute to the unpredictable nature of the maximum principal stress. The response of polymers to stress can involve phenomena such as strain hardening, stress relaxation, and creep, leading to variations in the stress distribution (Fried, 2014).

5. Conclusions

The presence of residual stresses in additively manufactured parts is a critical concern with practical implications. These stresses can introduce dimensional distortion, reduce mechanical properties, and even contribute to premature failure of the components. Therefore, understanding and controlling residual stresses is crucial for ensuring the quality, reliability, and functionality of FFF printed parts in various applications.

This dissertation has focused on the study of the influence of printing parameters on the residual stresses present in printed parts using Fused Deposition Modelling technology. Through a comprehensive Design of Experiments, three printing parameters were systematically varied to investigate their effects on residual stress formation.

The findings of this study have underscored the critical role of two key printing parameters: extrusion temperature and feed rate. These parameters exhibited the most substantial influence on residual stresses, as their interaction yielded notable effects on both the minimum and maximum principal stresses. Furthermore, the temperature-independent term and the square of the feed rate term demonstrated significance when analysing the results pertaining to the minimum principal stress. The extrusion temperature, as an indicator of the thermal history of the specimen, played a pivotal role in determining the magnitude and distribution of residual stresses. Additionally, the feed rate, representing the speed at which material is deposited, significantly affected the stress distribution within the printed part.

An innovative aspect of this research was the utilization of virtual extensometers, through digital image correlation. The strains calculated through the averages within predefined areas produced results closer to those obtained using physical strain gages, however they also appear to be more susceptible to DIC processing errors. Although not as accurate as traditional strain gauges due to factors such as sub-ideal distribution of the speckle pattern and slight hole displacements in relation to the stationary camera between hole increments, virtual extensometers offered a promising alternative for measuring small displacements on the specimen surfaces. The non-contact measurement capability of the Hole drilling-DIC technique, coupled with its convenience, and reduced preparation time are advantageous for analysing residual stress behaviour in FFF printed parts.

In conclusion, this dissertation has shed light on the influential role of printing parameters on the formation of residual stresses in FFF printed parts. The application of virtual extensometers has demonstrated potential as an alternative measurement technique. As additive manufacturing continues to advance, it is imperative to continue investigating, understanding, and effectively managing residual stresses to ensure the optimal performance and reliability of FFF printed components across various industries. Further research in this field will undoubtedly contribute to the advancement and wider adoption of this additive manufacturing technology.

5.1. Future work

Further research on the influence of printing parameters on residual stresses in Fused Deposition Modelling printed parts holds significant potential for advancing the understanding, optimization, and application of this additive manufacturing technology. This may include the research of additional printing parameters, since while this study focused on extrusion temperature, layer height and feed rate, there are numerous other printing parameters that can influence residual stress formation. Exploring the effects of factors such as bed temperature and flow rate would provide valuable insights into their contributions to residual stress behaviour. A comprehensive Design of Experiments considering a wider range of printing parameters would help establish a more complete understanding of their individual and combined effects.

Developing advanced numerical models and simulations can also aid in predicting and optimizing residual stress distribution in FFF printed parts. Incorporating material models that account for the viscoelastic behaviour and thermal history of the polymer material would enhance the accuracy and reliability of predictions. Coupling these models with computational fluid dynamics simulations to account for the complex flow behaviour during the extrusion process would further refine the understanding of residual stress formation mechanisms.

Investigating the influence of different materials on residual stress formation could also be an important area of research. Comparing the behaviour of various polymer materials commonly used in FFF printing, such as PLA and ABS with PETG would provide insights into their inherent material properties and their effects on residual stress formation. Additionally, exploring the impact of incorporating additives, fillers, or reinforcements in the filament formulation on residual stress behaviour would be valuable for optimizing material selection and achieving desired mechanical properties.

In conclusion, the study of the influence of printing parameters on residual stresses in FFF printed parts offers numerous avenues for further research. Advancing our understanding of the underlying mechanisms, optimizing printing parameters, developing advanced modelling techniques, and validating predictions through experiments will contribute to the continuous improvement and wider adoption of FFF additive manufacturing technology. By addressing these research directions, we can enhance the quality, reliability, and performance of FFF printed parts, opening up new opportunities for their use in various industries.

References

ANSYS. Ansys GRANTA EduPack software, Inc., Cambridge, UK, (www.ansys.com/materials). 2022.

ASTM E837-13. Standard Test Method for Determining Residual Stresses by the Hole-Drilling Strain-Gage Method. ASTM International, 2013. 10.1520/E0837-13

Bijak-Zochowski, M. A semi-destructive method of Measuring Residual Stresses, Internationale Konferenz Experimentelle Spannungsanalyse, Munich,
VDI Berichte, vol. 313, pg. 469-476. 1978.

Chu, T., Ranson, W., Sutton, M., Peters, W. Application of Digital Image Correlation Techniques to Experimental Mechanics, Experimental Mechanics, vol. 25 (3), 232-244. 1985. https://doi.org/10.1007/BF02325092

Correlated Solutions. VIC-2D Digital Image Correlation. (no date) Accessed May 30, 2023. https://www.correlatedsolutions.com/vic-2d.

DONG, P., BRUST, F. W. Welding residual stresses and effects on fracture in pressure vessel and piping components: a millennium review and beyond. J. Pressure Vessel Technol. 122.3: 329-338. 2000. https://doi.org/10.1115/1.556189

Filipe Oliveira Braga, D., & Manuel Salgado Tavares de Castro, P. Contour Method: Procedure Optimization. 2012.

Flaman, M. T. and Manning, B. H. Determination of Residual Stress Variation with Depth by the Hole-Drilling Method, Exp. Mech., vol. 25, No. 3, pg. 205-207. 1985. https://doi.org/10.1007/BF02325088

Fried, J.R. Polymer Science and Technology. Upper Saddle River, NJ: Prentice Hall. 2014.

Gao, X., Yu, N., & Li, J. Influence of printing parameters and filament quality on structure and properties of polymer composite components used in the fields of automotive. In *Structure and Properties of Additive Manufactured Polymer Components* (pp. 303–330). Elsevier. 2020. https://doi.org/10.1016/B978-0-12-819535-2.00010-7.

Guessasma, S., Belhabib, S., & Nouri, H. Printability and tensile performance of 3D printed polyethylene terephthalate glycol using fused deposition modelling. *Polymers*, *11*(7). 2019. https://doi.org/10.3390/polym11071220

Hamidi, A., & Tadesse, Y. Single step 3D printing of bioinspired structures via metal reinforced thermoplastic and highly stretchable elastomer. *Composite Structures*, *210*, 250–261. 2019. https://doi.org/10.1016/j.compstruct.2018.11.019

Holcomb, G., Caldona, E. B., Cheng, X., & Advincula, R. C. On the optimized 3D printing and post-processing of PETG materials. *MRS Communications*, *12*(3), 381–387. 2022. https://doi.org/10.1557/s43579-022-00188-3

Manufactur3d. *How does the FDM 3D Printing Technology Work?*. (2018, January 29). Available at:https://manufactur3dmag.com/working-fdm-3d-printing-technology/ (Accessed: April 24, 2023).

Minitab. *Interpret the key results for analyse response surface design.* (no date) Available at: https://support.minitab.com/en-us/minitab/21/help-and-how-to/statistical-modeling/doe/how-to/response-surface/analyze-response-surface-design/interpret-the-results/key-results/#step-2-determine-whether-the-association-between-the-response-and-the-term-is-statistically-significant (Accessed: 01 June 2023).

James, M. R., Lu, J., Handbook of Measurement of Residual Stresses, Edit. Jian Lu, The Fairmont Press, Inc. United States, 1996. DOI: 10.5860/choice.34-2182

Jankovic, A., Chaudhary, G., & Goia, F. Designing the design of experiments (DOE) – An investigation on the influence of different factorial designs on the characterization of complex systems. *Energy and Buildings*, *250*. 2021. https://doi.org/10.1016/j.enbuild.2021.111298

Johnson, Gregory. Residual stress measurements using the contour method. PhD thesis, Faculty of Engineering and Physical Sciences, University of Manchester, 2008.

Kelsey, R. A., Measuring Non-Uniform Residual Stresses by the Hole Drilling Method, Proc. SESA, No. 1, 1956, pg. 181-194. https://doi.org/10.1115/1.3226060

Kirsch, G., Theory of Elasticity and Application in Strength of Materials, Zeitchrift Vevein Deutscher Ingenieure, 42, No. 29, 1898, pg. 797-807.

Lacarac, V.; Smith, D.J.; Pavier, M.J.; Priest, M. Fatigue crack growth from plain and cold expanded holes in aluminium alloys. Int. J. Fatigue 2000, 22, 189–203. https://doi.org/10.1016/S0142-1123(99)00126-7

Lu, J., Flavenot, J. F., Trials in Increasing the Precision of the Incremental Hole-Drilling Method for Residual Stresses Distribution Determination, Residual Stresses, in Science and Technology, Int. Conf. on Residual Stress 1986, Germany.

Mason, R. L., Gunst, R. F., & Hess, J. L. (n.d.). Statistical Design and Analysis of Experiments with Applications to Engineering and Science Second Edition, 2003. 10.1002/0471458503

Mathar, J., Determination of Initial Stresses by Measuring the Deformation around Drilled Holes, Trans. ASME, 56, 1934, pg. 249-254. https://doi.org/10.1115/1.4019712

Mohan, D., Teong, Z. K., Bakir, A. N., Sajab, M. S., & Kaco, H. Extending cellulose-based polymers application in additive manufacturing technology: A review of recent approaches. In *Polymers* (Vol. 12, Issue 9). 2020. MDPI AG. https://doi.org/10.3390/POLYM12091876

Moreno Nieto, D., Casal López, V., & Molina, S. I. Large-format polymeric pellet-based additive manufacturing for the naval industry. *Additive Manufacturing*, *23*, 2018, 79–85. https://doi.org/10.1016/j.addma.2018.07.012

Neto, D. M., Borges, M. F., Sérgio, E. R., & Antunes, F. v. Effect of Residual Stresses on Fatigue Crack Growth: A Numerical Study Based on Cumulative Plastic Strain at the Crack Tip. *Materials*, *15*(6). 2022. https://doi.org/10.3390/ma15062156

Nickola, W. E., A Practical Subsurface Residual Stress Evaluation by the Hole-Drilling Method, Proc. 1986 SEM Spring Conf. on Exp. Mech., June 8-13, New Orleans, pg. 47- 58, SEM, Bethel, CT (1986).

Niku-Lari, A. Lu, J., Flavenot, J. F., Measurement of Residual Stress Distribution by the Incremental Hole-Drilling, Exp. Mech., vol. 25, No. 2, 1985, pg. 175-185. https://doi.org/10.1016/0378-3804(85)90023-3

Nobre, J. P., Sobre o comportamento mecânico de camadas superficiais dos materiais: estudo do contacto no impacto elasto-plástico; determinação do estado de tensões residuais pela técnica do furo incremental, PhD Thesis, Faculty of Science of the University of Coimbra, Coimbra, 2000. http://hdl.handle.net/10316/1695

Nobre, J. P., Kornmeier, M., Dias, A. M., Scholtes, B., Use of the Hole-drilling Method for Measuring Residual Stresses in Highly Stressed Shot-peened Surfaces, Experimental Mechanics, 40 (3), 2000, pg. 289-297. https://doi.org/10.1007/BF02327502

Papanikos, P., Mechanics of Mixed Mode Fatigue Behaviour of Cold Worked Adjacent Holes, thesis for Doctor of Philosophy, University of Toronto, Toronto, 1997.

Piloto, P.A.G; Vila Real, Paulo; Mesquita, Luís; Vaz, M.A.P., Steel Mechanical Properties Evaluated At Room Temperature After Being Submitted At Fire Conditions, Proc., XXX IAHS - World Congress on Housing Construction, 2002, pg. 1545-1553. http://hdl.handle.net/10198/2039

Rendler, N. J. and Vigness, I., Hole-Drilling Strain-Gage Method of Measuring Residual Stresses, Experimental Mechanics, 6, No. 12, 1966, pg. 577-586. https://doi.org/10.1007/BF02326825

Ribeiro, J.E.P.C, Caracterização Experimental e Numérica de Campos de Tensões Residuais Provocadas por Processos de Fabrico, tese de doutoramento, Faculdade de Engenharia da Universidade do Porto, Porto, 2006

Schajer, G. S., Application of Finite Element Calculations to Residual Stress Measurements, J. Eng. Mater. Tech., 4, vol. 103, 1981, pg. 157-163. https://doi.org/10.1115/1.3224988

Schajer, G. S., Measurement of Non-Uniform Residua Stresses Using the Hole-Drilling Method, Part I – Stresses Calculation Procedures, J. Eng. Mater. Technology, vol. 110, No. 4, 1988, pg. 338-343. https://doi.org/10.1115/1.3226059

Sint Technology. MTS3000-Restan EVAL software - Operating and maintnance manual. (no date)

Sint Technology. MTS3000 - Restan - Sint Technology - Residual Stress Analyzer. January 27, 2021. https://www.sintechnology.com/products/mts3000-restan/.

Slotwinski, J.A., Additive Manufacturing: The Current State of the Art and Future Potential, Johns Hopkins APL Technical Digest, Volume 35, Number 4, 2021, www.jhuapl.edu/techdigest

Soete, W. and Vancrombrugge, R., An Industrial Method for Determination of Residual Stress, Proc. SESA, No. 1, 1950, pg. 17-18.

Soete, W., Measurement and Relaxation of Residual Stress, Sheet Met. Ind., No. 266, 1949, pg. 1269-1281.

Teixeira, Óscar, Francisco J. G. Silva, Luís P. Ferreira, and Eleonora Atzeni. A Review of Heat Treatments on Improving the Quality and Residual Stresses of the Ti–6Al–4V Parts Produced by Additive Manufacturing, 2020, Metals 10, no. 8: 1006. https://doi.org/10.3390/met10081006

Vishay Precision Group. Tech Note TN-503: Measurement of Residual Stresses by the Hole-Drilling* Strain Gage Method. 1993.

Wong, Kaufui V., and Aldo Hernandez. A Review of Additive Manufacturing. ISRN Mechanical Engineering, 2012. https://doi.org/10.5402/2012/208760.

Annex A: Results of the Principal Stresses of the Specimens

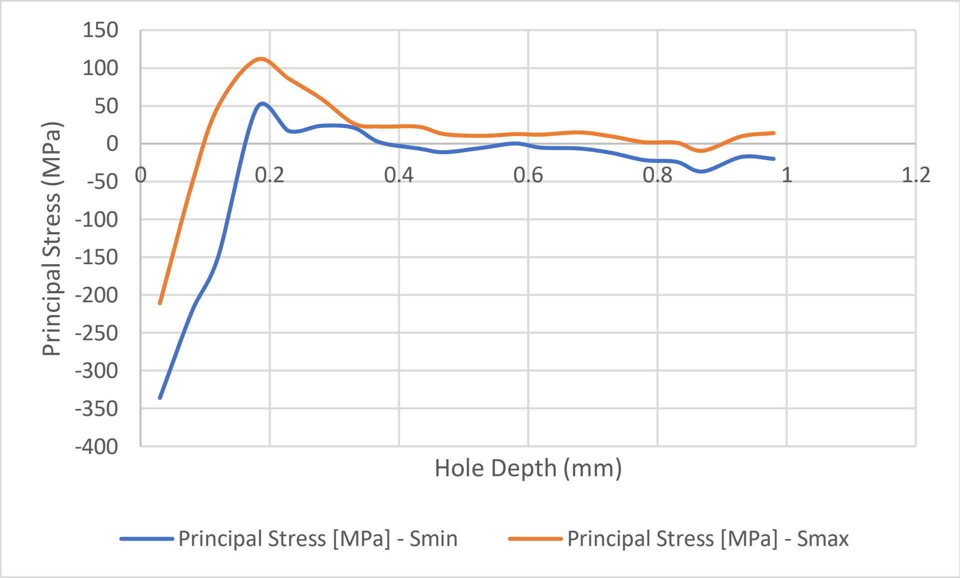

Figure 41 - Principal Stresses measured in Specimen 3

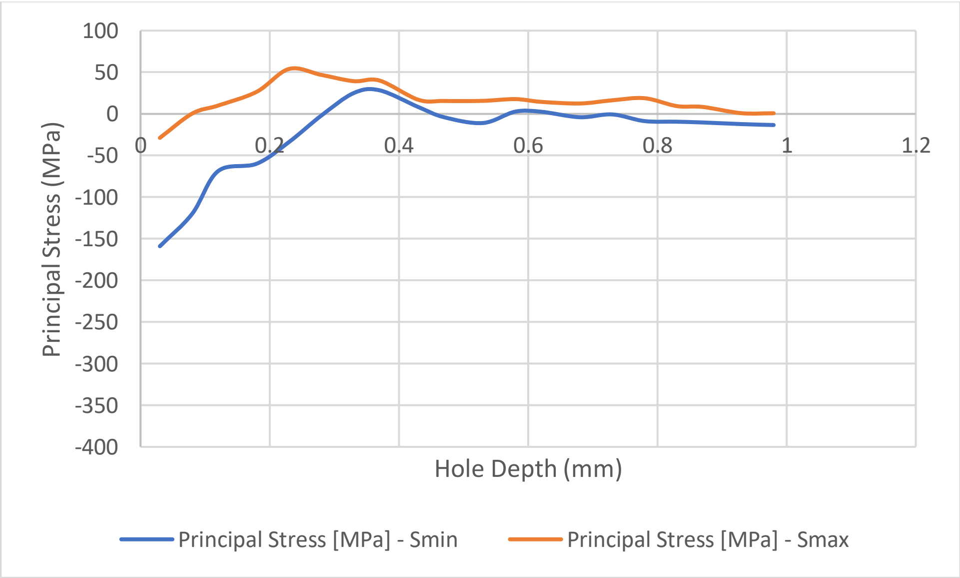

Figure 42 - Principal Stresses measured in Specimen 4

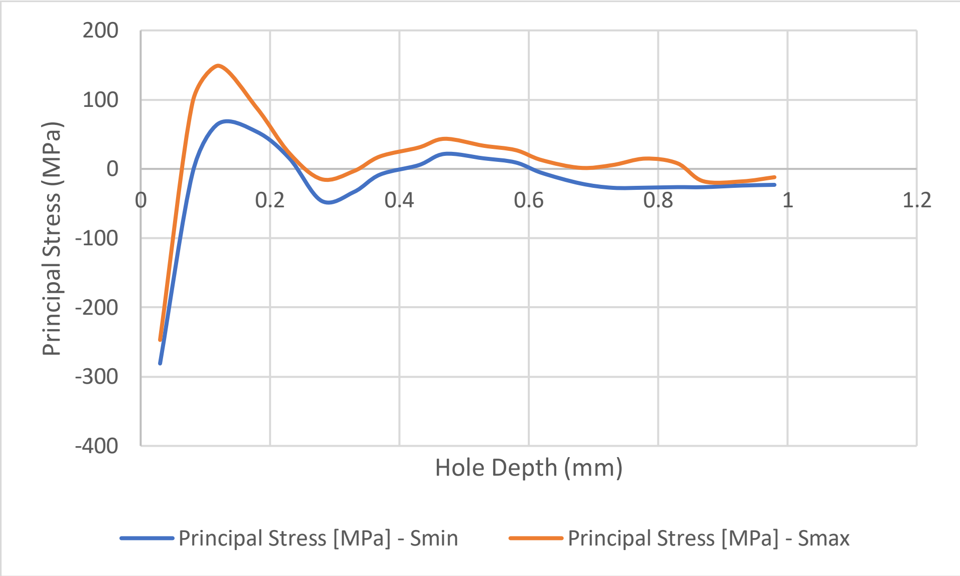

Figure 43 - Principal Stresses measured in Specimen 5

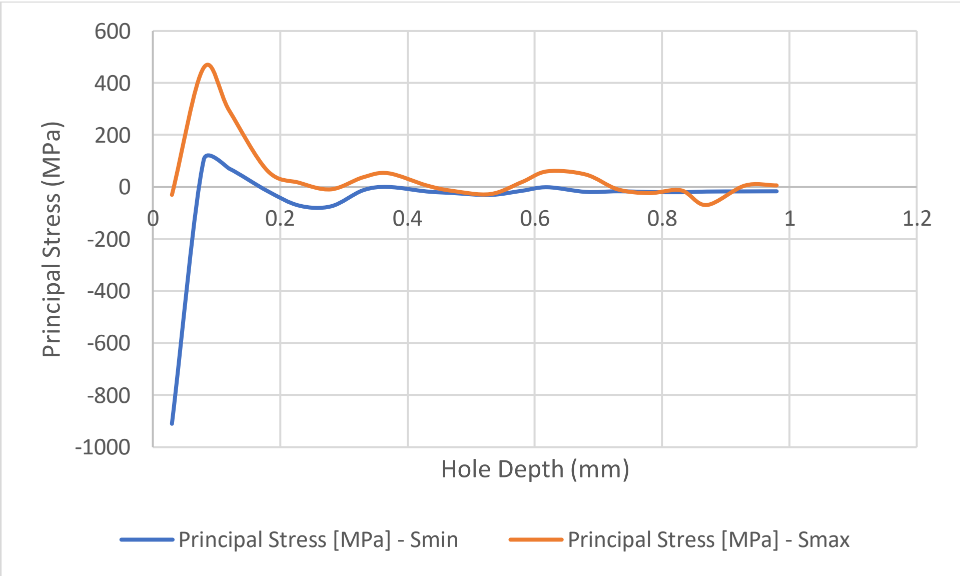

Figure 44 - Principal Stresses measured in Specimen 6

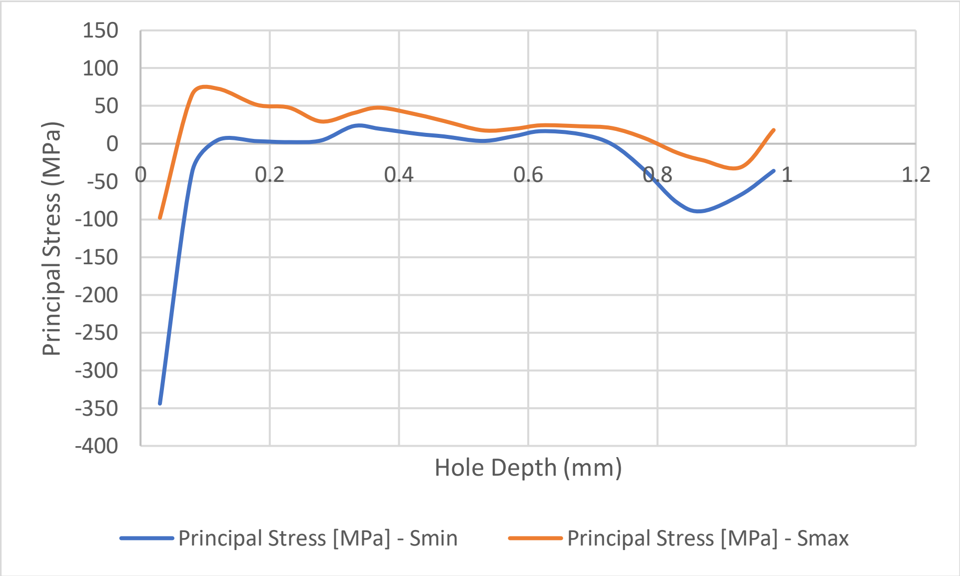

Figure 45 - Principal Stresses measured in Specimen 7

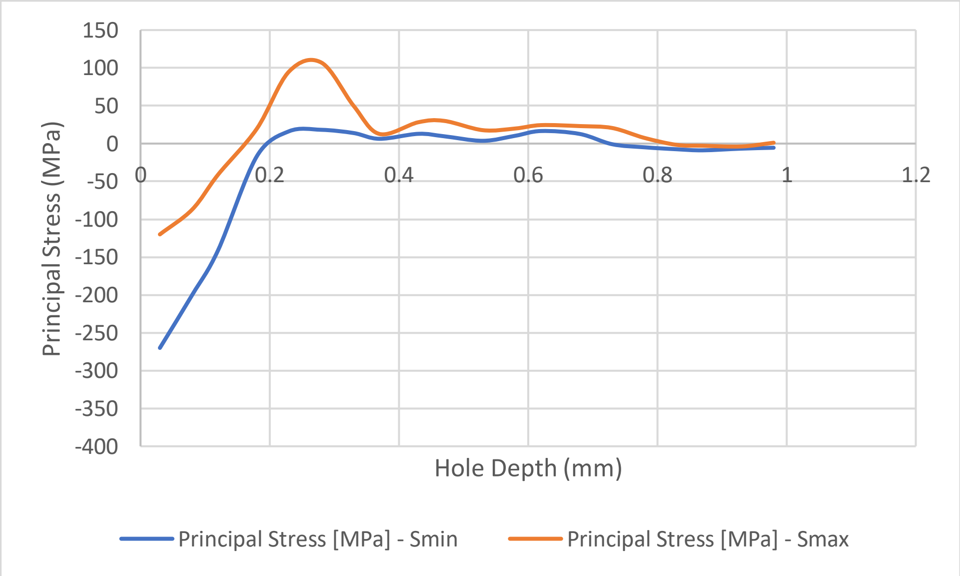

Figure 46 - Principal Stresses measured in Specimen 8

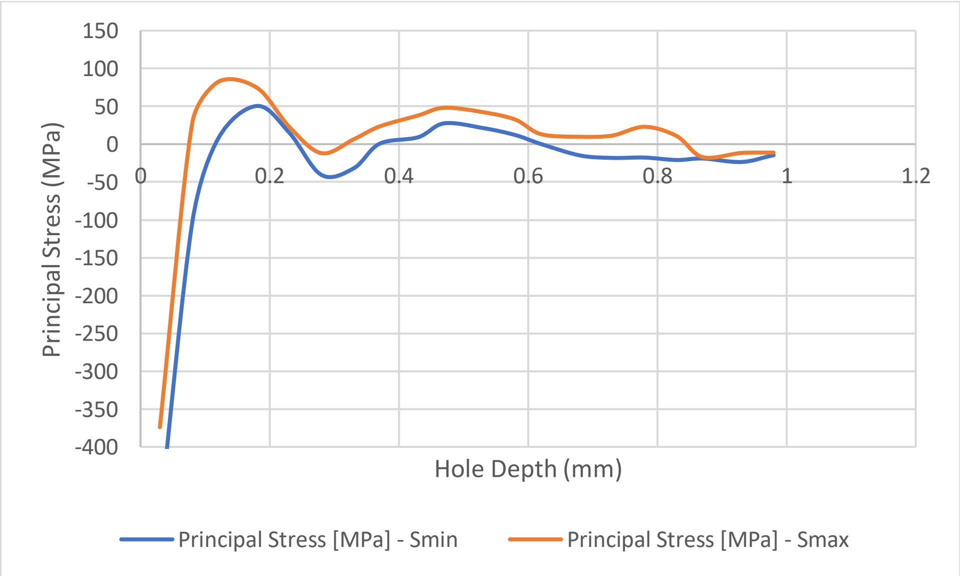

Figure 47 - Principal Stresses measured in Specimen 9

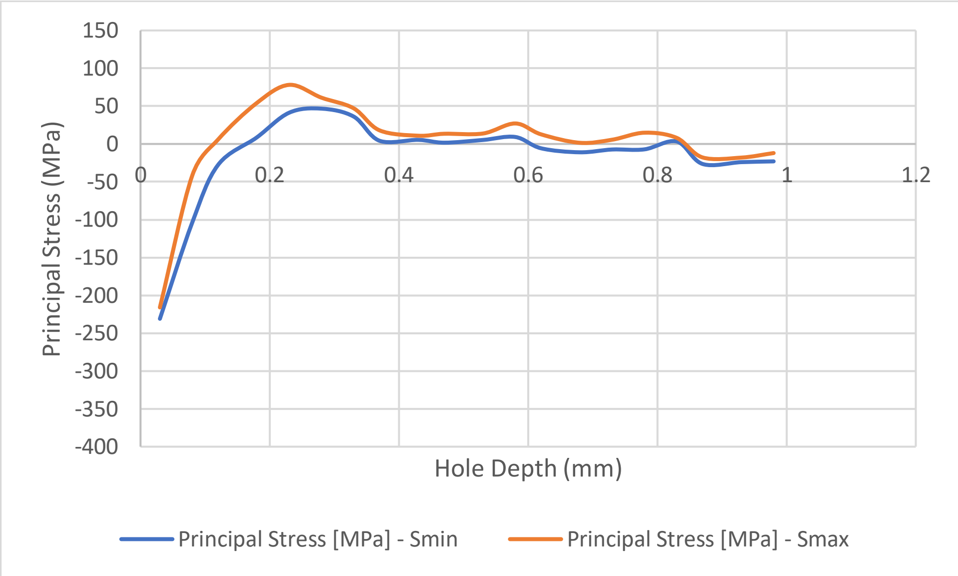

Figure 48 - Principal Stresses measured in Specimen 10

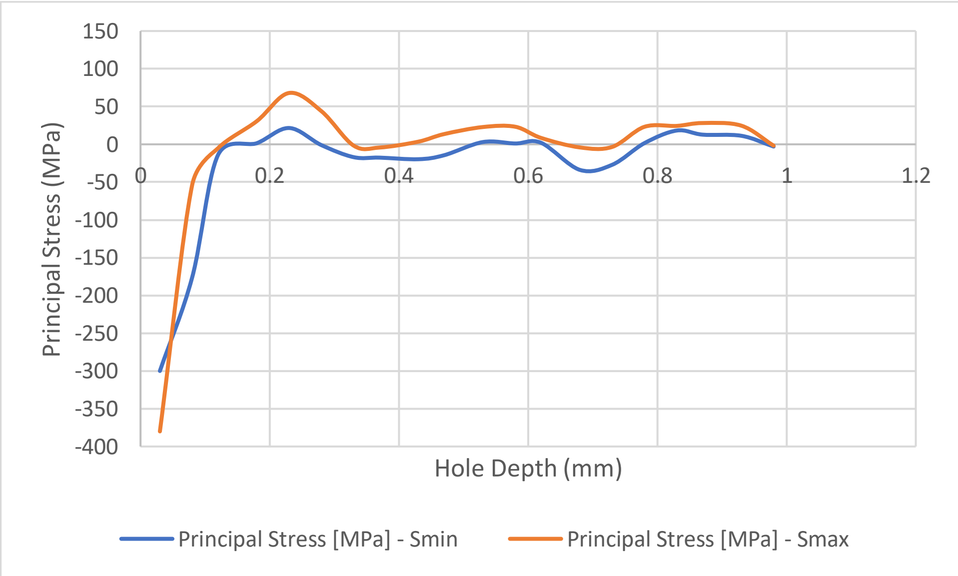

Figure 49 - Principal Stresses measured in Specimen 11

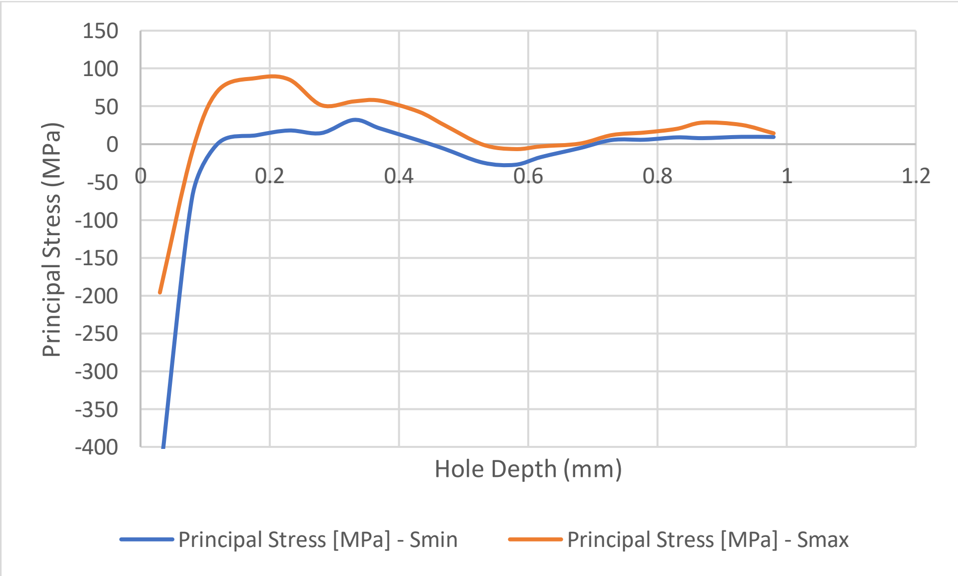

Figure 50 - Principal Stresses measured in Specimen 12

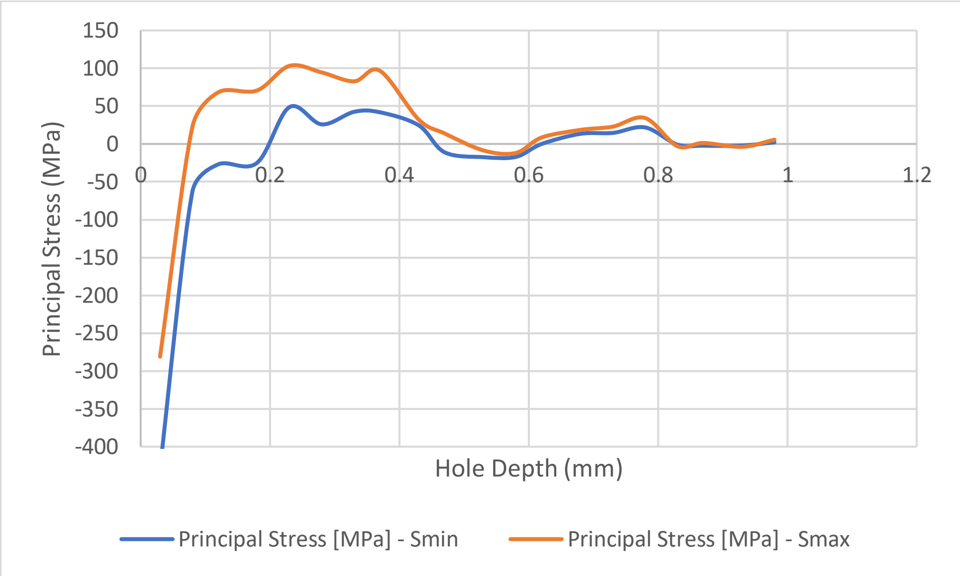

Figure 51 - Principal Stresses measured in Specimen 13

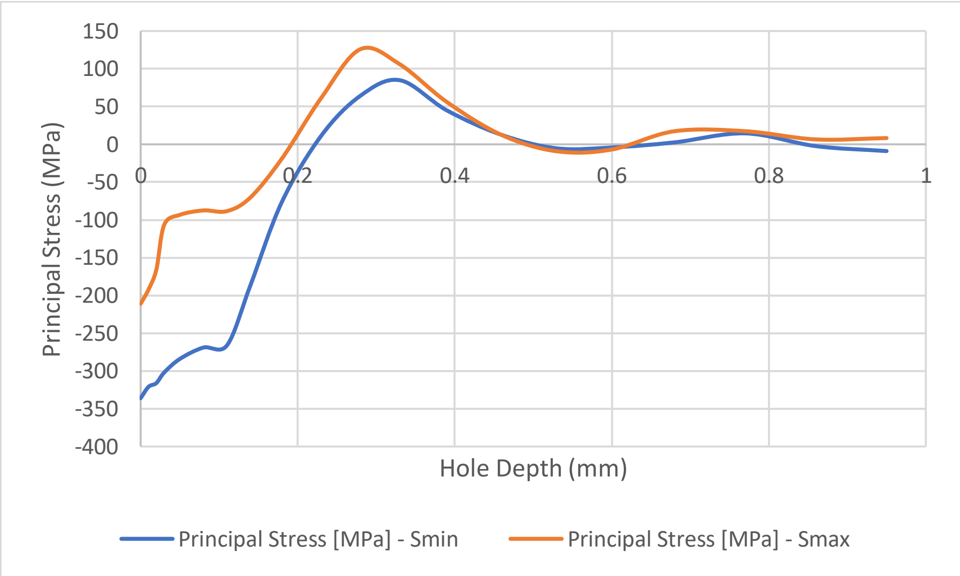

Figure 52 - Principal Stresses measured in Specimen 14

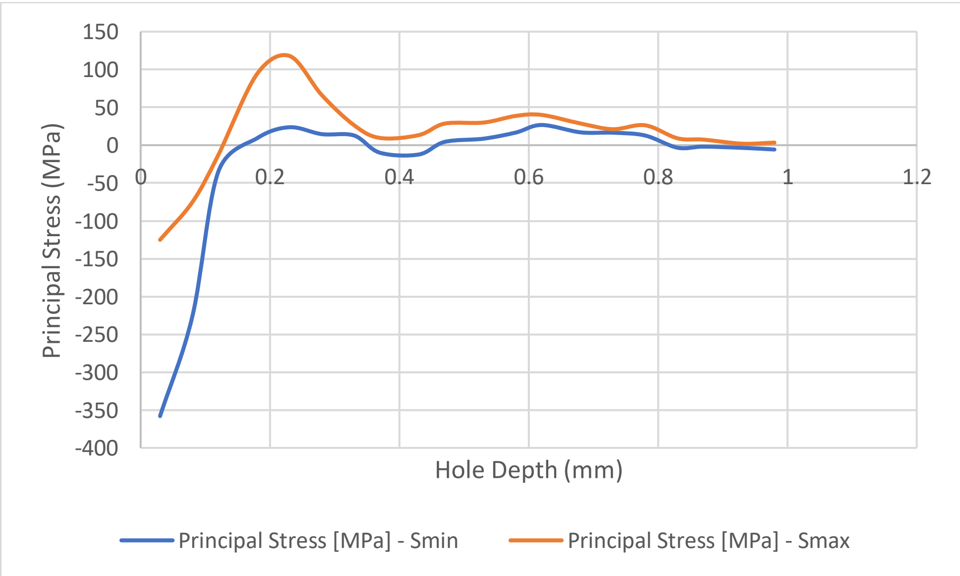

Figure 53 - Principal Stresses measured in Specimen 15

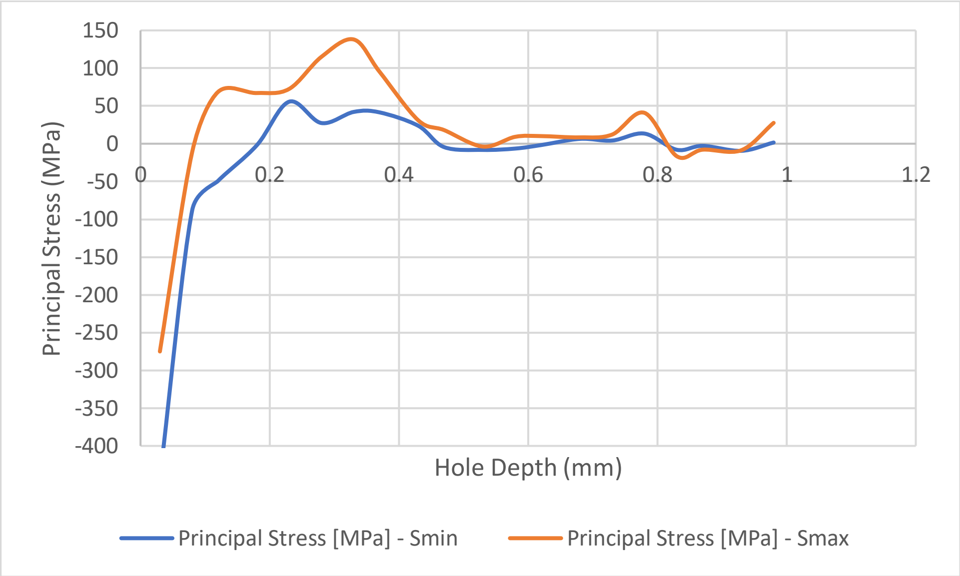

Figure 54 - Principal Stresses measured in Specimen 16

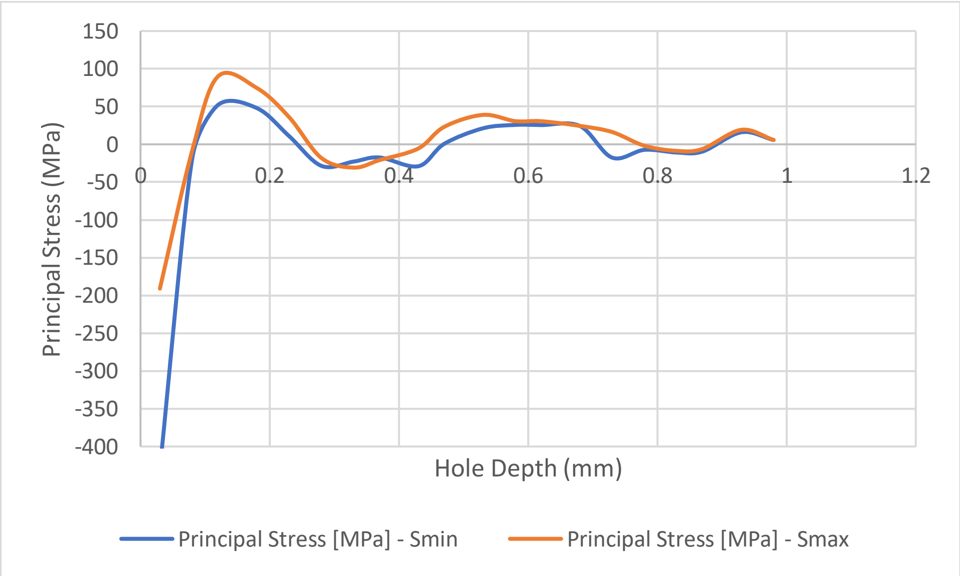

Figure 55 - Principal Stresses measured in Specimen 17

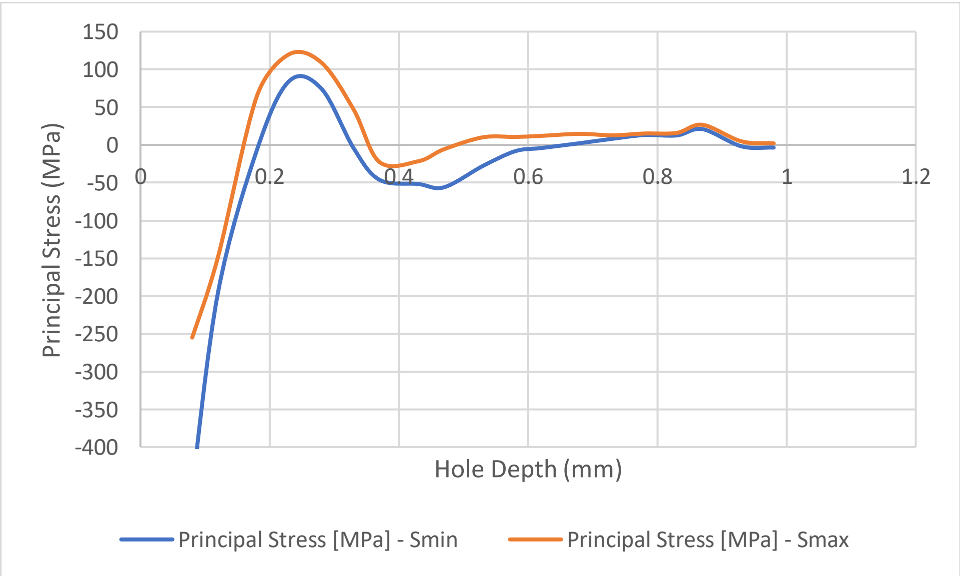

Figure 56 - Principal Stresses measured in Specimen 18

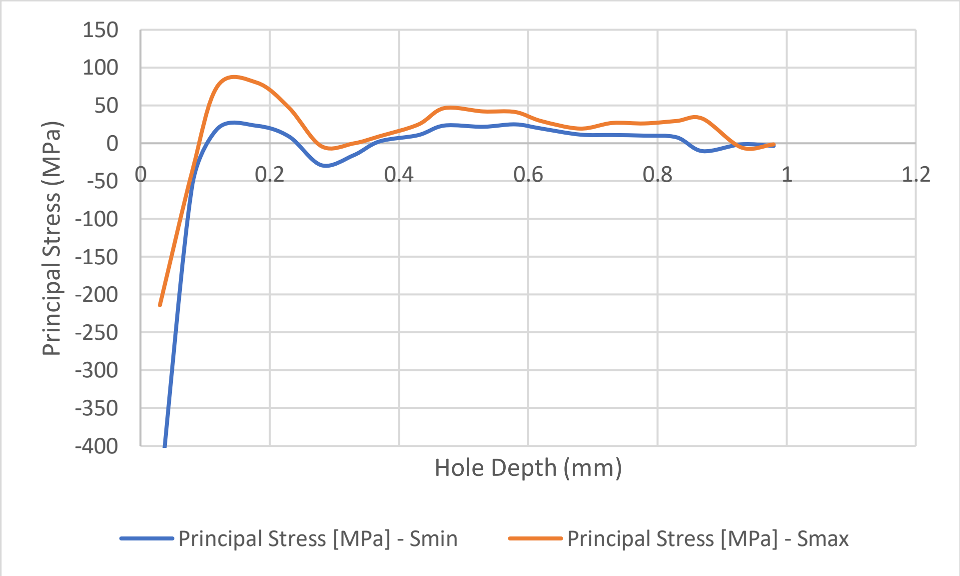

Figure 57 - Principal Stresses measured in Specimen 19

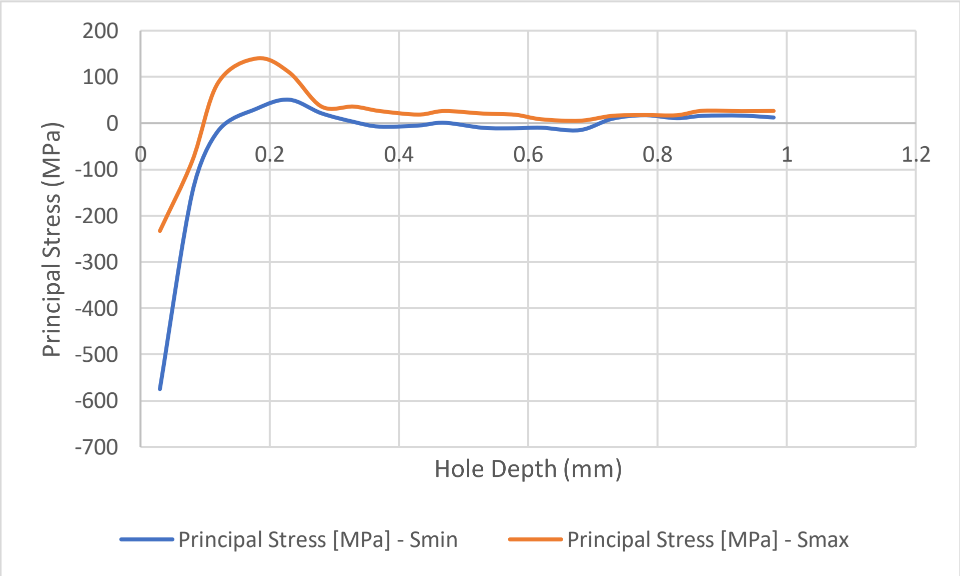

Figure 58 - Principal Stresses measured in Specimen 20